



NRL/MR/7540--07-9080

An Assessment of the Meteorological Conditions Leading to the NOAA WP-3D Engine Compressor Stalls of February 9, 2007, Due to Sea Salt Aerosol Particle Fouling

JEFFREY S. REID
CDR DANIEL P. ELEUTERIO, USN
B. JOHN COOK
ANNETTE L. WALKER
KIM A. RICHARDSON
DOUGLAS L. WESTPHAL
JIANGLONG ZHANG

*Meteorological Applications Development Branch
Marine Meteorology Division*

A. BARRY DAMIANO
RICHARD J. McNAMARA
MARTIN MAYEAUX

*National Oceanographic and Atmospheric Administration
Aircraft Operations Center
Tampa, Florida*

October 25, 2007

Approved for public release; distribution is unlimited.

REPORT DOCUMENTATION PAGE

Form Approved
OMB No. 0704-0188

Public reporting burden for this collection of information is estimated to average 1 hour per response, including the time for reviewing instructions, searching existing data sources, gathering and maintaining the data needed, and completing and reviewing this collection of information. Send comments regarding this burden estimate or any other aspect of this collection of information, including suggestions for reducing this burden to Department of Defense, Washington Headquarters Services, Directorate for Information Operations and Reports (0704-0188), 1215 Jefferson Davis Highway, Suite 1204, Arlington, VA 22202-4302. Respondents should be aware that notwithstanding any other provision of law, no person shall be subject to any penalty for failing to comply with a collection of information if it does not display a currently valid OMB control number. **PLEASE DO NOT RETURN YOUR FORM TO THE ABOVE ADDRESS.**

1. REPORT DATE (DD-MM-YYYY) 25-10-2007		2. REPORT TYPE Memorandum Report		3. DATES COVERED (From - To) April 1 – July 15, 2007	
4. TITLE AND SUBTITLE An Assessment of the Meteorological Conditions Leading to the NOAA WP-3D Engine Compressor Stalls of February 9, 2007, Due to Sea Salt Aerosol Particle Fouling				5a. CONTRACT NUMBER	
				5b. GRANT NUMBER	
				5c. PROGRAM ELEMENT NUMBER	
6. AUTHOR(S) Jeffrey S. Reid, CDR Daniel P. Eleuterio, USN,* B. John Cook, Annette L. Walker, Kim A. Richardson, Douglas L. Westphal, Jianglong Zhang, A. Barry Damiano, † Richard J. McNamara, † and Martin Mayeaux †				5d. PROJECT NUMBER	
				5e. TASK NUMBER	
				5f. WORK UNIT NUMBER	
7. PERFORMING ORGANIZATION NAME(S) AND ADDRESS(ES) Naval Research Laboratory Marine Meteorology Division, Code 7500 7 Grace Hopper Avenue, Stop 2 Monterey, CA 93907				8. PERFORMING ORGANIZATION REPORT NUMBER NRL/MR/7540--07-9080	
9. SPONSORING / MONITORING AGENCY NAME(S) AND ADDRESS(ES) Office of Naval Research, Code 322MM Dr. Ronald Ferek 875 N. Randolph Street, Suite 1425 Arlington, VA 22203-1995				10. SPONSOR / MONITOR'S ACRONYM(S)	
				11. SPONSOR / MONITOR'S REPORT NUMBER(S)	
12. DISTRIBUTION / AVAILABILITY STATEMENT Approved for public release; distribution is unlimited.					
13. SUPPLEMENTARY NOTES *NRL Code 7000 †NOAA Aircraft Operations Center, Tampa, FL					
14. ABSTRACT This report presents our findings from a meteorological analysis of NOAA WP-3D N42RF engine compressor stalls of February 9, 2007, which nearly led to the loss of the aircraft. Preliminary engineering and meteorological analysis performed by the National Atmospheric and Oceanic Administration (NOAA) pointed to sea salt fouling when the aircraft encountered super concentrations of sea salt aerosol particles in the atmosphere at altitude above 1 km. To our knowledge, this type of sea salt event is previously unrecorded in the peer-reviewed literature. Utilizing a combination of model, satellite, and in situ data we tracked the flight environment for three research flights as part of the 2007 Ocean Winds Winter Experiment (OWWE) out of St. John's, Newfoundland, where the aircraft experienced hurricane force winds. Questions addressed include what conditions can lead to super concentrations of sea salt in the marine atmosphere and in particular why was there a failure on the February 9 flight and not on others. In this particular case, the aircraft track took it into the dry slot behind the bent-back warm-type occluded front of a North Atlantic explosive cyclogenesis event. In this environment, dry polar air is advected at high wind speeds over the relatively warm waters of the Gulf Stream. This led to an environment of high winds, high seas, and massive atmospheric instability and turbulence along a 400 km fetch without precipitation. This allowed giant sized sea salt particles to be well mixed in the marine boundary layer. By our estimations, marine boundary layer heights for this flight were on the order of 1200 to 1500 m, well above the flight level of the aircraft. In comparison, other OWWE flights may have experienced high winds, but not the other causal factors determined for February 9. Lastly, since the WP-3D was intersecting warm, moist, and sea salt laden updrafts in between longer periods of drier environments, it is possible that increased sea salt accretion developed through the oscillating wet-dry cycle. We conclude this report with meteorological and operational guidance.					
15. SUBJECT TERMS Severe weather Aviation operations Sea salt					
16. SECURITY CLASSIFICATION OF:			17. LIMITATION OF ABSTRACT	18. NUMBER OF PAGES	19a. NAME OF RESPONSIBLE PERSON
a. REPORT	b. ABSTRACT	c. THIS PAGE			Jeffrey S. Reid
Unclassified	Unclassified	Unclassified	UL	39	19b. TELEPHONE NUMBER (include area code) (831) 656-4725

CONTENTS

1.0 EXECUTIVE SUMMARY	1
2.0 INTRODUCTION: THE INCIDENT OF FEBRUARY 9, 2007, AND RATIONALE FOR THIS REPORT	2
3.0 FUNDAMENTALS OF SEA SALT PRODUCTION AND TRANSPORT	6
4.0 ANALYSIS OF METEOROLOGICAL CONDITIONS FOR OWWE	12
5.0 SUMMARY METEOROLOGICAL GUIDANCE AND AVAILABLE PRODUCTS TO ASSESS SEA SALT CONDITIONS.....	30
6.0 SUMMARY RECOMMENDATIONS.....	33
7.0 ACKNOWLEDGMENTS	34
8.0 REFERENCES.....	35

1.0 EXECUTIVE SUMMARY

On February 9, 2007, the NOAA WP-3D aircraft N42RF lost power to three of its four engines over the northern Atlantic Ocean during moderately low level (~800 m) flight in a hurricane force wind region. These failures left insufficient power for sustained flight and the WP-3D crew prepared to perform an in-water emergency landing. Fortunately, after passing through a minor one-minute long rain band, pilots were able to restart the engines and return home safely. A preliminary investigation suggested that sea salt aerosol particles generated in the high winds and high (up to 20 m) seas coated the aircraft and caused severe engine fouling resulting in compressor stalls. NOAA's original assessment suggested that the brief rain band experienced by the aircraft washed off sufficient salt to help aid the pilots in restarting the engines.

As part of an incident investigation, NOAA officially requested the assistance of the Naval Research Laboratory (NRL) Marine Meteorology Division to help understand the meteorological conditions that led to the event. Specific questions posed to NRL included:

- a) What were the meteorological conditions that led to the extreme airborne sea salt particle loadings experienced by the WP-3D?
- b) Where and how often do these conditions take place? Are they predictable?
- c) At first assessment, the conditions experienced by the February 9 flight were similar to others during this campaign in which there was no incident. Can the meteorological data explain this difference?
- d) What recommendations and guidance can NRL provide to help ensure flight safety?

The extreme events that led to the massive salt concentrations encountered by the WP-3D are not uncommon but are rarely experienced, as most pilots try to avoid such weather phenomena if predicted, unless the mission requires it, as this airborne research did. In this particular case, the WP-3D flight track took it through the dry slot of an occluding storm system which had just completed a period of explosive cyclogenesis. This particular sector of a storm sometimes experiences very high wind speeds and seas but little precipitation. Consequently, sea salt concentration built up rapidly but was not scavenged by precipitation. Furthermore, the dynamics of this intensifying occluded system led to a deep marine boundary layer (MBL), which was higher than the mission flight level (over 1 km). Other environmental conditions, such as a moist-dry cycle, may have led to additional salt accretion on the aircraft.

There is very little collected data on sea salt aerosol particles in high wind conditions, and much of the data at moderate wind speeds is suspect, but the existing literature is reviewed here and available data sets are composited to derive a more complete picture. Much of this analysis relies on the U.S. Navy's Coupled Ocean/Atmosphere Mesoscale Prediction System–On Scene (COAMPS-OS[®]) with which special model runs were performed for this study.

Guidance here only requires a qualitative understanding of the system, as the primary causal factors for the environmental conditions experienced are determined to be a lack of wet scavenging by precipitation, and high surface marine winds, both of which can be found in the dry slot of intense extra-tropical cyclones. WP-3s may experience extreme sea salt conditions in the marine boundary layer top in a region of non-precipitating, high-wind ($>25 \text{ m s}^{-1}$) conditions for prolonged time periods. By carefully observing the atmospheric state variables measured on the WP-3D, the boundary layer height (and hence the salt layer) should become apparent. The NRL Aerosol Analysis and Prediction System (NAAPS), the U.S. Navy's operational global aerosol forecast model, which has shown skill in predicting sea salt concentrations, can also be used to provide numerical guidance.

2.0 INTRODUCTION: THE INCIDENT OF FEBRUARY 9, 2007, AND RATIONALE FOR THIS REPORT

On February 9, 2007, at approximately 20:20 Z while flying at an altitude of ~800 m, the National Oceanic and Atmospheric Administration (NOAA) WP-3D research aircraft N42RF lost power to three of its four engines approximately 500 nautical miles from land over the Atlantic Ocean [NOAA, preliminary report to be published 2007]. Conditions experienced by N42RF at that time can be described as hurricane-like, with winds of 90+ kts (45 m s^{-1}) and 60+ ft seas (20 m). A WP-3D cannot remain airborne with power from only one engine, and immediately began to descend. As crew prepared to ditch the aircraft, pilots managed to restart the three engines and bring the aircraft safely back to base.

Upon investigation it was determined that the power failure was caused by excess buildup of sea salt aerosol particles within N42RF's Rolls Royce engines. However, during the millions of hours flown by P-3 type aircraft, only once before had a power failure ever been documented to be induced by sea salt; a NOAA WP-3D lost power to one engine in 2003 during the Coupled Boundary Layer Air-Sea Transfer (CBLAST) experiment while flying at low level in between rain bands of a hurricane. Indeed, as part of this particular field study, N42RF had repeatedly flown in similar conditions without incident. The pending question then is "Why was there a failure on this particular flight and not others?"

In a letter dated April 18, 2007, CAPT Philip W. Kenul, commanding officer of the NOAA Aircraft Operations Center, requested the Naval Research Laboratory's assistance in assessing the meteorological conditions leading to the mishap. The letter also requested help or guidance in predicting similar situations to help safeguard future missions.

This memorandum report has been generated in response to this official NOAA request. The analysis was supported by an Office of Naval Research Code 322MM sponsored research program on aerosol prediction. Here we compile and present relevant meteorological and satellite data regularly archived by the NRL Marine Meteorology Division and perform an analysis of the meteorological conditions during the event. Using the U.S. Navy's Coupled Ocean/Atmosphere Mesoscale Prediction System—On Scene (COAMPS-OS[®]), simulations were performed to closely examine the boundary layer structure. Using these data sets, we have developed guidance regarding the situations that can produce extreme sea salt aerosol particle concentrations at moderately high altitudes. We conclude with a list of commonly available on-line tools that may help NOAA flight planning when such environments may exist.

2.1 The events of February 9, 2007

It is educational to recount the events leading to the incident in question. Here a short synopsis is presented. However, a more detailed description is available in the official incident report performed by NOAA, from which this is drawn. The research flight in question was being performed as part of the 2007 Ocean Winds Winter Experiment (OWWE) out of St. John's, Newfoundland. Performing calibration/validation flights for satellite-based microwave surface winds retrievals, N42RF frequently flew into hurricane-like conditions with 65+ kts (32 m s^{-1}) surface winds and heavy seas at an altitude of 800–1000 m. On February 9, 2007, at 18:23 Z (15:00 LST), N42RF launched from its base at St. John's to measure winds behind a rapidly developing cyclone due south of Greenland at latitude 45 N longitude 40 W. Figure 1 presents the flight track for this mission overlaid on the 21:00 Z SEVERI IR image with Navy Operational Global Atmospheric Prediction System (NOGAPS) forecast surface wind speeds (in knots).

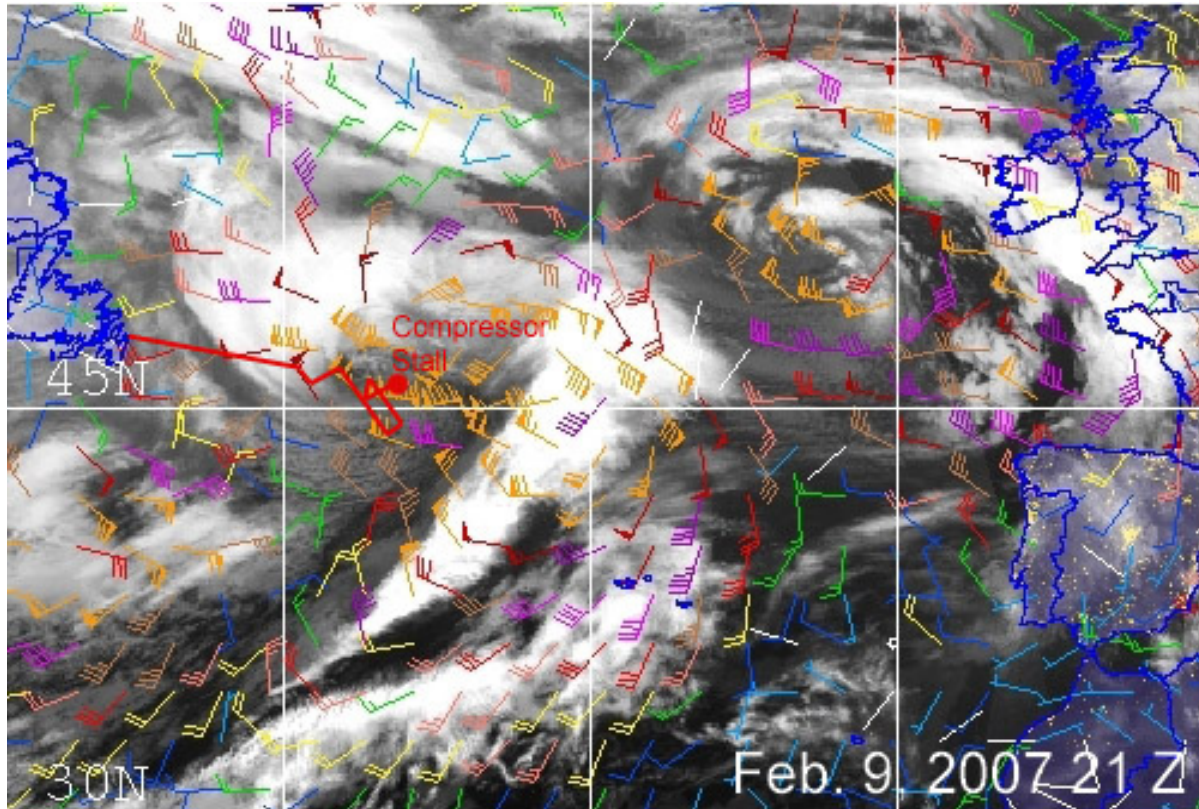


Figure 1. Meteosat-8 (MSG)-SEVERI infrared image of the northern Atlantic Ocean for 21 Z, February 9, 2007. Included are the Navy Operational Global Atmospheric Prediction System (NOGAPS) forecast surface wind barbs (in knots). Overlaid in red is the flight track of the aircraft including the point of compressor stalls. In the vicinity of the incident, NOGAPS analyzed 90+ knot winds.

At approximately 20:00 Z the flight track took N42RF through the low center of an intense occluding cyclone where, on the east side, winds reached 90–95+ kts ($>45 \text{ m s}^{-1}$). The last dropsonde was deployed at 22:20 Z at 830 m altitude. As the aircraft crew collected data from the final release and prepared to return to base, crew noticed flames emanating from the #3 engine tailpipe followed by a high Turbine Inlet Temperature (TIT) warning light, but no fire warning horn. The pilot and flight engineer conducted emergency shutdown procedures on engine #3, and increased power to #1, #2, and #4 engines. Before emergency shutdown procedures could be conducted on #3, crew members then reported flames on #4, again with an increase in TIT but no warning horn. Scientific data systems shut down at 22:21:50 Z when the #4 engine shut down.

Now conducting emergency shutdown in #3 and #4, power was cautiously further increased to #1 and #2 and N42RF began to climb. But, in order to maintain 200 knot airspeed and engine integrity, N42RF descended to 800 m. Four minutes later, fire was reported on #1. After an attempt to reduce the flames, #1 was also shut down. Unable to retain altitude on one engine, N42RF began to descend at 220 m/min and emergency radio broadcasts were sent and crew donned their exposure suits.

Pilots initiated a restart of engine #1 and it was at this point that N42RF encountered a brief rain shower. After reaching a minimum altitude of 275 m the engine was restarted and N42RF began a slow climb. Eventually engines #3 and #4 were also restarted. N42RF returned to base at 4500 m altitude without further notable incident. During the return flight leg and after landing, crew noticed an

excessive amount of sea salt accretion on the aircraft, particularly on engine inlets. After landing, engines were covered pending further investigation.

The final report from Rolls Royce engineers suggested that the engine shutdowns were due to the accretion of sea salt aerosol particles on the compressor stator and rotor blades, which resulted in deformation of the intake airflow and consequently reduced efficiency and ultimately caused compressor stall. It is unknown how much engine efficiency was regained by the brief flight period in the rain shower while the engines were being restarted. Engineers further cautioned that salt accretion can occur during high wind periods in the absence of liquid precipitation at altitudes higher than 400 m and that mission planning should consider this phenomenon.

2.2 The cases of January 22 and February 8, 2007

In addition to information regarding the flight of February 9, NOAA provided data on two other flights conducted as part of the 2007 Ocean Winds Winter Experiment which experienced similar wind speeds but did not result in engine power loss. Most important, N42RF flew a similar pattern in seemingly comparable conditions less than 20 hours earlier with a takeoff time of 22:00 Z on February 8 (henceforth referred to as the F8 flight). The incident of February 9 (henceforth F9) was a storm that was part of a pair of similar intense cyclogenesis events spawned by a parent low over Newfoundland. The flight of February 8 is used here as a case study that showed similar development. The flight track for the February 8 flight is presented in Figure 2(a). (Note this storm can be viewed in Figure 1 twenty-four hours later at latitude 47 N and longitude 18 W.)

The second event examined in this report took place on January 22, 2007 (henceforth the January 22 flight, or J22). Unlike the intense cyclogenesis events of February 8 and 9, in this case N42RF flew along the leading edge of a powerful trough (Figure 2(b)). Here too, winds were high, measured in excess of 90 kts at flight level (~800 m).

2.3 Rationale for this Memorandum Report

As will be described in the remainder of this report, the conditions leading to engine power loss, while not uncommon globally, are rarely experienced. Consequently, there are limited atmospheric data sets collected in such conditions, and virtually no sea salt aerosol particle measurements available in the scientific community. Indeed, upon discussion of this case with colleagues, none had ever heard of a sea salt layer in such massive concentrations and large particles existing as high as the flight level of N42RF on February 9. The purpose of this report is not only to provide a record of the meteorological conditions leading to the incident, and guidance for future missions, but also to provide scientific examination of the development of these unique environmental conditions.

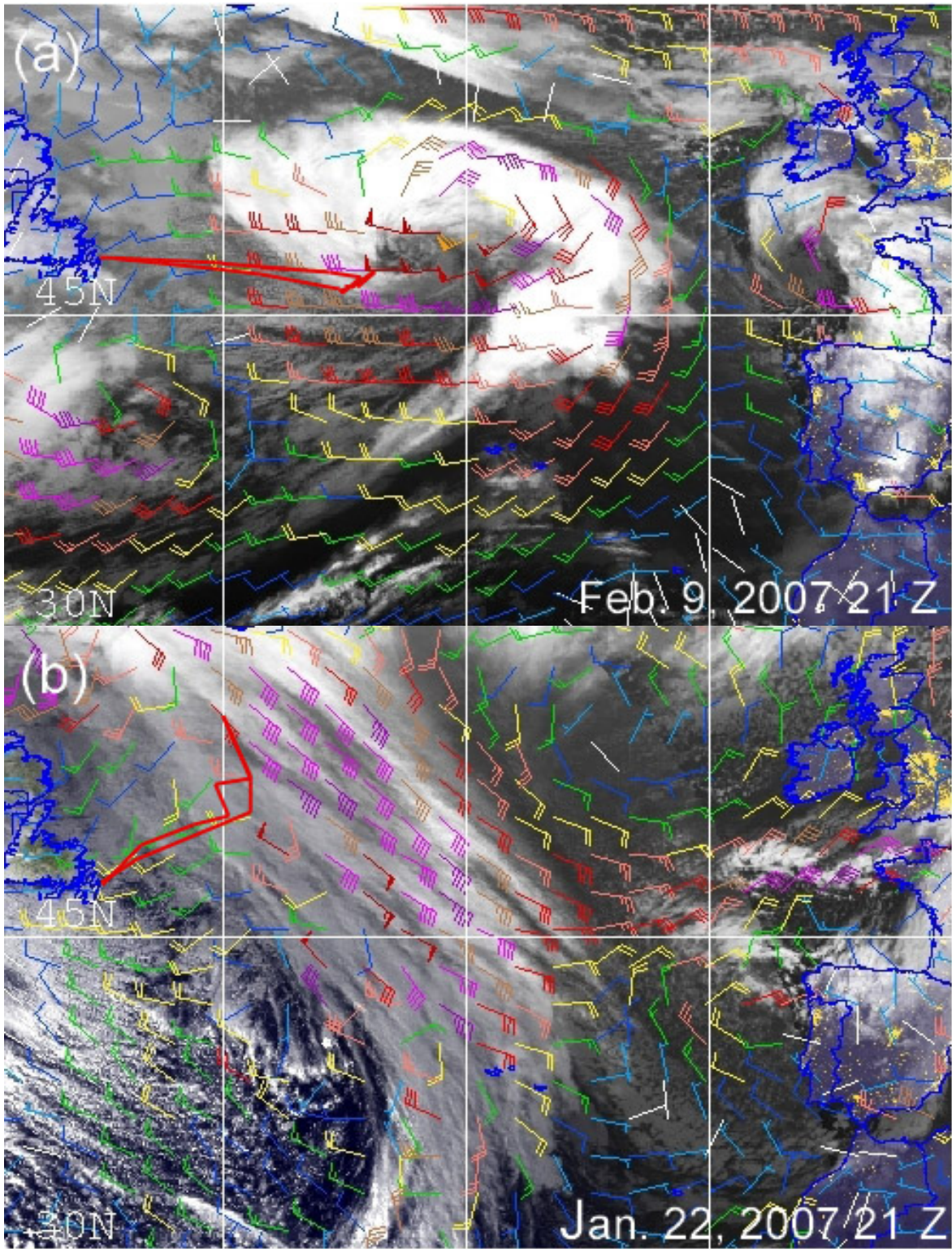


Figure 2. Same as Figure 1, but for (a) the flight with takeoff at ~18:00 Z February 8, 2007 (image 00 Z February 9), and (b) the flight of January 22, 2007.

3.0 FUNDAMENTALS OF SEA SALT PRODUCTION AND TRANSPORT

A complete review of the production and transport of sea salt particles from the ocean surface can be found in the review manuscript of *Fitzgerald* [1991] and the monograph by *Lewis and Schwartz* [2004]. However, for context we present a brief overview here of issues that significantly impact our analysis.

Historically, of all aerosol species, the study of sea salt and marine aerosol particles on naval systems has understandably received the most attention by Navy-sponsored research. However, despite the significant amount of Navy and civilian study and our qualitative understanding of the topic, there is still much scientific debate regarding many of the most fundamental processes. For example, it has been repeatedly shown that measurements of wind-speed-dependent sea salt concentrations and sea spray fluxes reported in the literature vary by several orders of magnitude [e.g., *Andreas* 1998; *Lewis and Schwartz* 2004]. Several metastudies such as *Porter and Clarke* [1997], Table 3 from *Reid et al.* [2001] and Figure 4 of *Smirnov et al.* [2003] have found that reported volume median diameters (VMDs) varied by over a factor of five. Even the application of fundamental processes such as sea salt production and dry deposition has come increasingly into question [e.g., *Reid et al.* 2001; *Hoppel et al.* 1989; *Lewis and Schwartz* 2004]. This uncertainty is compounded with the community's realization that the wind-whitecap relationship is highly variable with such additional independent variables as wind/wave direction, sea surface temperature (SST), and chemistry [*Terrill et al.* 2001; *Martensson et al.* 2003].

Despite these uncertainties, however, a qualitative understanding of sea salt geochemical cycles and transport has emerged. Both fine mode (aerosol particle diameter $d_p < 2.5 \mu\text{m}$) and coarse mode ($2.5 < d_p < 15 \mu\text{m}$) sea salt are produced by the bursting of air bubbles at the surface of the ocean during whitecapping. These particles have relatively low settling velocities and can persist in the absence of precipitation in the marine atmosphere for hours to days (an hour for $15 \mu\text{m}$ particles), to over a week for fine mode particles. In addition to these bubble bursting aerosol particles, larger droplets of ocean water can be ejected from the center of a bursting bubble (or jet drop) or torn from the froth that forms the crests of waves, forming a giant mode ($d_p > 200 \mu\text{m}$) known as spume drops. These particles are typically rather short lived in the atmosphere, lasting from seconds to minutes. In the following subsections we discuss the nature of these sea salt aerosols in the marine boundary layer.

3.1 Sea Salt Aerosol Particle Size

There is a great deal of variability in the reported size distribution of salt particles. Some of this variability in salt-particle fluxes and size distributions is due to variations in wind speed and wave height [*Blanchard et al.* 1984; *Hoppel et al.* 1989; *Fitzgerald* 1991; *Porter and Clarke* 1997]. However, most of the measurements presented in the scientific literature may be flawed and suffer from significant measurement bias [*Reid et al.* 2006; *Reid and Peters* 2007]. Further, the influence of relative humidity (RH) on sea salt particle size (i.e., the particle's *hygroscopicity*) is not a constant, as previous thought, but rather is strongly influenced by organic mass fractions of the ocean water and ocean surface as well as secondary organic species generated photochemically in the atmosphere [*Crahan et al.* 2004].

The bulk of the literature on sea salt and spray concerns the nature of coarse mode sea salt particles. These particles can have atmospheric lifetimes from hours to days, and receive their attention due to their significance in the fields of atmospheric chemistry and cloud microphysics. For film/bubble bursting particles, it currently appears that sea salt droplets have a volume median diameter on the order of 5 μm at a relative humidity of 80%. This is approximately twice the size of a dry pure sea salt particle, and half the size it would be at the time of production where the relative humidity is $\sim 98\%$ [Tang *et al.* 1997]. Sea salt aerosol particles are mostly water in typical marine atmospheres and are in rapid equilibrium with relative humidity (less than a second to equilibrate). The influence of organic chemical species in the sea water, however, tends to reduce this hygroscopicity curve, with some of the more aged sea salt particles having their hygroscopic growth reduced by more than 25% [Crahan *et al.* 2004; Randles *et al.* 2004].

The much larger spume particles are even more difficult to characterize than those from smaller bubble burst production and have received considerably less study by the scientific community. First, while bubble bursting production occurs during any whitecap event (winds $>7 \text{ m s}^{-1}$), significant spume production occurs only at higher wind speeds (winds $>13 \text{ m s}^{-1}$ [Smith *et al.* 1993]). At these wind speeds and associated sea conditions, the physical measurement process becomes very difficult. For very high wind speeds (winds $>30 \text{ m s}^{-1}$), such measurements are almost nonexistent in the peer-reviewed literature.

There are a few fundamental measurements sets on spume-produced sea salt aerosol particles [e.g., Wu *et al.* 1984; Smith *et al.* 1993; deLeeuw 1990]. Even if measurements are uncertain with respect to size and concentration, they do at least sufficiently describe a few important points. Near the ocean surface (where all of these measurements have been made), the volume concentration of giant spume far outstrips that of coarse mode bubble bursting counterparts by several orders of magnitude. The spume production probably generates a volume modal diameter on the order of 100–200 μm . But at 10 m, the volume modal diameter would be $\sim 25\text{--}50 \mu\text{m}$ for particles lasting more than a minute.

Figure 3(a) presents measurements of sea salt aerosol particle size distributions taken offshore of Duck, North Carolina, in March 1999 from the Center for Interdisciplinary Remotely Piloted Aircraft Studies (CIRPAS) Twin Otter aircraft. Here the volume distributions from a wing-mounted forward scattering spectrometer probe (FSSP-100) for four cases of onshore flow with winds varying from 5 to 14 m s^{-1} [Reid *et al.* 2001] are presented. First, it must be emphasized that FSSP-100 instruments have a tendency to oversize particles in the 3–12 μm range. Hence, the 10 μm peak observed in this graph should physically be located around 5 μm , with a factor of eight decrease in volume. Regardless, the increase in particle concentration with wind speed is clearly visible. A better demonstration of the true size of coarse mode sea salt particles can be seen in Figure 3(b), where ambient sea salt size distributions are extrapolated from dry surface measurements based on the thermodynamic curves of Tang *et al.* [1997]. Here we can see the variability in sea salt particle size, ranging from 5 μm for 80% relative humidity (typical for the ocean surface), to near 9 μm for RH values found near the top of the marine boundary layer.

What is more interesting, though, from Figure 3(a) is not the coarse mode, but the development of the tail of the spume mode beginning at approximately 12 μm for the 14 m s^{-1} wind speed. From this plot, its magnitude seems to rival that of the coarse mode, taking into account the sizing error of the coarse mode by FSSP-like instruments; however, the giant mode (loosely defined as $>10 \mu\text{m}$) quickly dominates the volume distribution for these high wind speeds.

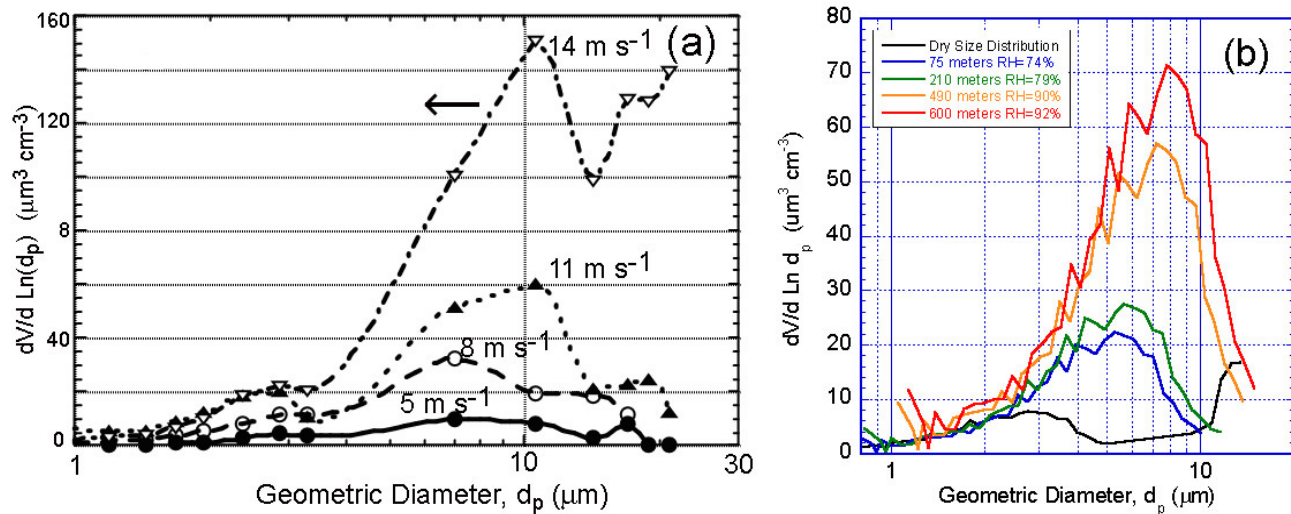


Figure 3. Measurements of sea salt particle volume distributions as a function of altitude above the sea surface. (a) Particle volume distributions measured offshore of Duck, North Carolina, using a wing mounted FSSP-100 particle probe (adapted from Reid *et al.* [2002]). Note that due to the response function of this type of instrument, it over-sizes coarse mode particles. Hence, the 10 μm mode should really be at 5 μm . But giant particles ($d_p > 14 \mu\text{m}$) are sized correctly. (b) Sea salt size distribution as a function of relative humidity based on aerodynamic particle sizer data and hygroscopicity curves of Tang *et al.* [1997] (adapted from Reid *et al.* [2006]).

3.2 Sea Salt Aerosol Particle Vertical Distribution in the Marine Boundary Layer

Because there does not exist an aircraft-based method that can measure the size distribution of sea salt particles in their ambient state [Reid *et al.* 2006], there is almost no accurate quantitative data on the subject of sea salt size resolved vertical distribution in the literature. Indeed, even in field studies such as the Coupled Boundary Layer Air-Sea Transfer Experiment (CBLAST), the study of sea salt particles is strongly lacking [Black *et al.* 2007]. However, the data that does exist systematically leads to the conclusion that for particles less than 15 μm in diameter, the marine boundary layer is fairly well mixed. That is, the standard temperature and pressure particle concentration is independent with height, with the exception of right at the ocean surface during production. Thus, fine and coarse mode sea salt can be considered to extend in near equal concentrations up to the top of the marine boundary layer.

In contrast, the vertical distribution of large and giant sea salt particles depends heavily on the marine boundary layer height, which in turn is heavily influenced by shear turbulence, stability, and convection related to air-sea temperature differences [Fairall *et al.* 1983; Blanchard *et al.* 1984; Exton *et al.* 1986]. Marine boundary layer heights are generally measured on the order of 400–700 m. However, in areas of strong negative air-sea temperature differences (i.e., unstable), MBL heights, and hence sea salt, have been shown to extend up to 800 m. Capping cumulus clouds (which are not uncommon in these situations) can mix sea salt several hundred meters further. In comparison, the typical flight level of the WP-3D was on the order of 850 to 950 m.

Figure 4 presents sea salt vertical profile data taken offshore from the east coast of the United States in 1999 [Reid *et al.* 2001] as part of the CIRPAS Twin Otter flight campaign. Vertical profiles of

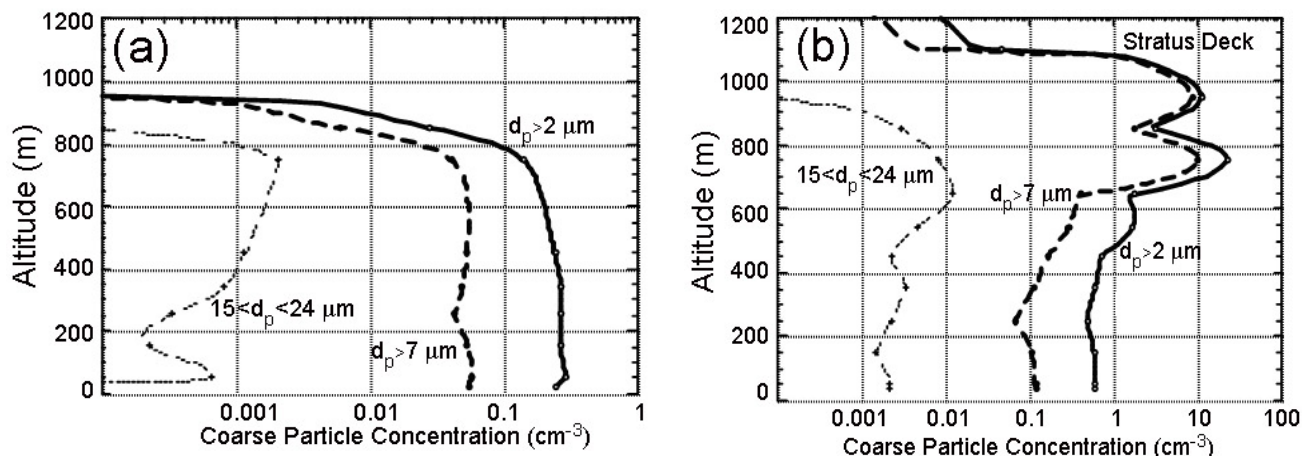


Figure 4. Vertical profiles of ambient coarse mode aerosol particle concentrations off the North Carolina coast during onshore flow using a FSSP-100 instrument on the CIRPAS Twin Otter [Reid *et al.* 2001]. (a) March 8, 1999, where winds were at 11 m s^{-1} . (b) March 11, 1999, over the Gulf Stream where winds were at 14 m s^{-1} .

particle number concentration were estimated using the FSSP-100. Again, while FSSP-like instruments greatly distort the size distribution and concentration of coarse mode aerosol particles [Reid *et al.* 2006], it does nevertheless qualitatively demonstrate the vertical extent of coarse mode particles such as sea salt. For the two cases presented, back trajectories suggested that these air masses had spent several days offshore. Because of the large extent of the Gulf Stream, the air mass must have spent time in unstable conditions that are frequent there.

Figure 4(a) presents the March 8, 1999, case where winds were approximately 11 m s^{-1} at the surface. Sea salt concentrations are shown to be relatively constant with height up to the top of the boundary layer at 800 m. This appears to be the case for particles up to $15 \mu\text{m}$ in size. However, for larger particles in the $15\text{--}24 \mu\text{m}$ range, concentrations appear to increase with altitude. This seemingly contradictory profile is a result of non-linearity in the FSSP-100 response function. In reality, because relative humidity increases with altitude in the MBL, particles grow in size. Hence, in a well mixed environment, ambient aerosol particle volume should also increase with height. In the case of the largest particles, the number concentration seemingly increases as particles grow into that size range.

The vertical extent of this marine boundary layer is likely enhanced due to its transport over the warm Gulf Stream. This can be further demonstrated in the second case presented in Figure 4(b) for March 11, 1999. This vertical profile was taken 150 km offshore over the Gulf Stream itself with surface wind speeds on the order of 14 m s^{-1} . The atmosphere was fairly unstable (air-sea temperature differences were on the order of -6° to -10°C), and even steam was observed leaving the ocean surface (“smoke on the water” phenomenon). The MBL in this case, however, was topped by a stratocumulus deck forced at the surface due to the high sea surface temperatures ($\sim 16^\circ \text{C}$). These non-precipitating clouds mixed sea salt aerosol particles to over 1 km.

Based on data from this same study, we can observe how quickly sea salt can be mixed to higher levels in Figure 5 [Reid *et al.* 2001]. For three flights, the CIRPAS Twin Otter flew profiles in the along-wind direction offshore of Duck, North Carolina. Three cases are shown in Figure 5. March 2

(Figure 5(a)) is a control case where winds were at 5 m s^{-1} and the atmosphere was thermodynamically neutral. Consequently, there was no sea salt production and little indication of an internal boundary layer, defined here as a non-equilibrium boundary layer associated with a discontinuity in surface forcing and rapid development, such as when (cold) continental air moves over (warm) water such as the Gulf Stream. In the March 1 case, however, surface winds were consistently at 8 m s^{-1} and a clear thermal internal boundary layer reaching 400 m is visible (Figure 5(b)). On March 4 (Figure 5(c)), winds were at 12 m s^{-1} . In this case, the internal boundary layer reached 700 m. For both these cases, maximum mixing heights occurred within 30 km of shore. It is also noteworthy that despite the March 4 case having 50% higher wind speeds, it did not result in higher particle concentrations. Column integrated sea salt was three times higher, but due to the higher boundary layer depth, particle concentrations were diluted. *Reid et al.* [2001] estimated that it would require another 100 km of transport before particle concentrations overtook those of the 8 m s^{-1} case.

3.3 Sea Salt Fluxes

The physical measurement of sea salt fluxes is probably one of the most difficult tasks in marine aerosol science. As discussed in *Andreas* [1998] and *Lewis and Schwartz* [2004], estimates of fluxes presented in the literature span several orders of magnitude, especially with regards to larger spume-generated particles. However, there is a general consensus that production flux and spume surface area likely scale to the cube of friction velocity [*Andreas* 1998]. Consequently, production flux is also then proportional to the cube of 10 meter wind speed. Thus, in higher wind regimes, even seemingly small increases in wind speed could result in significant increases in sea salt concentration.

Coarse mode sea salt particles have dry deposition velocities that allow them to remain airborne for hours to several days. Even for high wind conditions, when dry deposition velocities increase due to impaction, production will outstrip deposition and particles will be well mixed in the MBL. Hence in a precipitation-free atmosphere, coarse mode concentration will increasingly build until wind speeds substantially subside. Wet deposition, however, is a significant remover of coarse mode particles. While the exact efficiencies are open to scientific debate, the fact that the atmosphere is well cleansed of such particles is taken as a given [*Lewis and Schwartz* 2004].

For sea salt particles greater than approximately $10 \mu\text{m}$, dry deposition velocities typically dominate the deposition cycle and are closely linked to settling rates. For particles at 10, 15, 20, 30, and $40 \mu\text{m}$, settling velocities rapidly increase to 0.3, 0.7, 1.2, 2.7, and 4.8 m s^{-1} , respectively. For comparison, under more typical conditions, mid-boundary layer vertical velocity (w') values are on the order of 0.5 to 1 m s^{-1} . Hence, as we saw in Figure 4, particles up to $18 \mu\text{m}$ can likely remain aloft at wind speeds sufficient to create spume particles in the first place. As winds increase or as atmospheric stability decreases, this critical diameter will also increase, thus non-linearly increasing salt concentration at altitude. In the case of hurricane force winds as sampled by the WP-3D, mixing velocities probably exceed 5 m s^{-1} , corresponding to particles $40 \mu\text{m}$ in diameter.

The importance of dry deposition should not de-emphasize wet scavenging, however. Even for large sea salt particles with lifetimes on the order of an hour, precipitation will very effectively remove them from the atmosphere. For cases of high winds, high instability, and recent precipitation, the precipitation would prevent sea salt from mixing to the top of the MBL in any appreciable quantity.

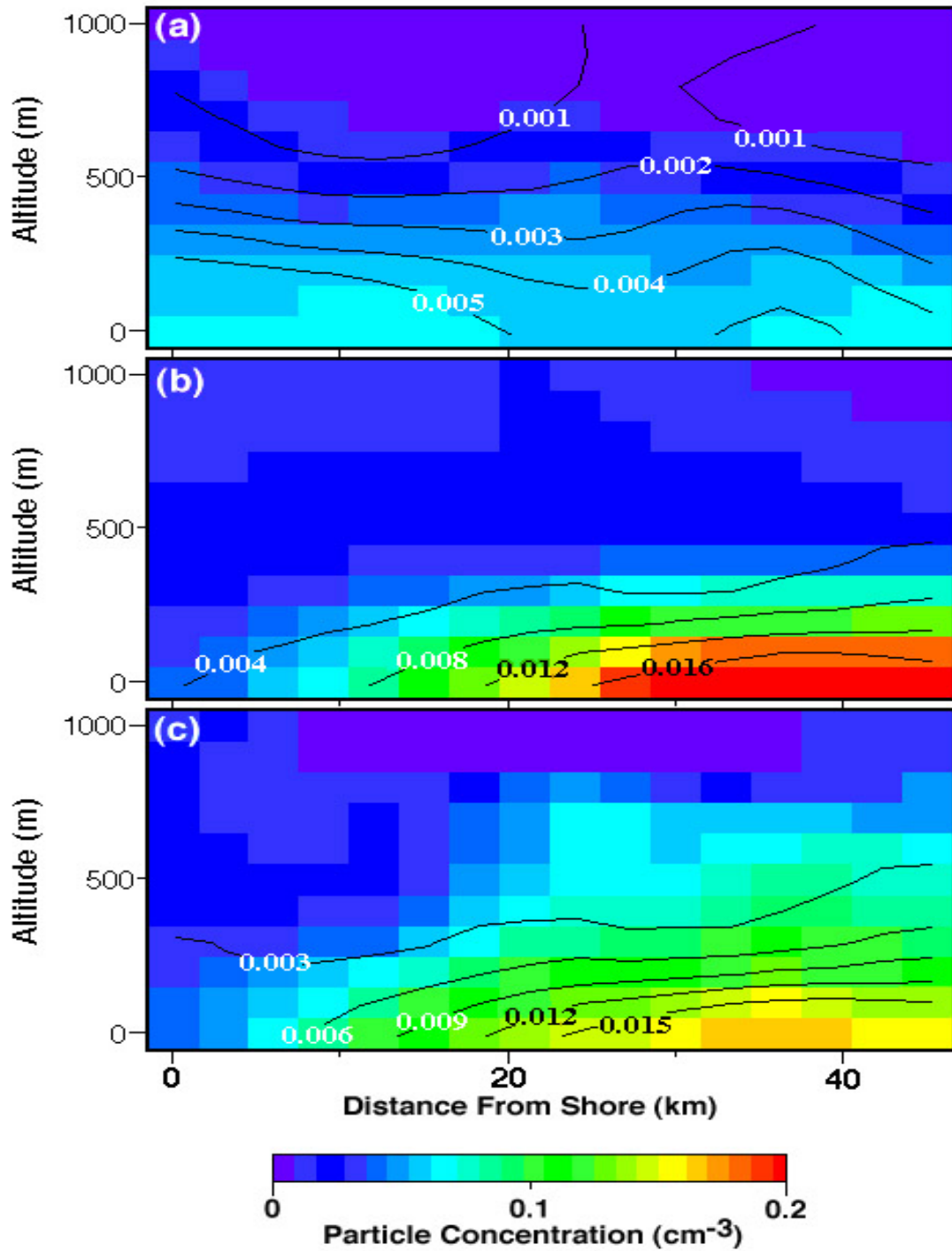


Figure 5. Nearshore 2D cross section of particle concentration in the coarse mode with diameters between $2\text{--}7\ \mu\text{m}$ (color), and giant mode with diameters between $7\text{--}16\ \mu\text{m}$ (isolines) for 3 days of offshore flow [Reid *et al.* 2001]. (a) March 2, $u = 5\ \text{m s}^{-1}$, (b) March 1, $u = 8\ \text{m s}^{-1}$, (c) March 4, $u = 12\ \text{m s}^{-1}$. Units are in cm^{-3} .

3.4 Implications for this Analysis

Based on the above review, there are several key points that have bearing on this investigation. First, we probably need to differentiate the impact of coarse and giant mode sea salt particles. Under most circumstances, giant sea salt particles from spume production are too heavy to reach much vertical extent. However, as seen in Figure 4, the tail of the spume production mode (particles less than, say, 15 μm) can definitely be mixed to the top of the MBL for moderate winds and unstable conditions. Once hurricane force winds are reached, or a combination of dry convection during unstable conditions coupled with shear-generated turbulence, it is quite possible that larger droplets up to $\sim 30 \mu\text{m}$ could mix to the top of the boundary layer. The critical size for such a phenomenon would be when mixing velocities exceed settling velocities. Even under more typical conditions, mid-boundary layer w' values are on the order of 0.5 to 1 m s^{-1} . This would correspond to a particle size on the order of 18 μm (and justifiable based on the profile shown in Figure 5). While we do not have particle sizing data, it is the hypothesis of this report's authors that it was these giant particles that caused the salt fouling event. Only particles in this size range are likely have the dry mass to coat the aircraft as photographed by the NOAA flight crew. In the following section, we will examine the meteorology of several WP-3D flights and determine if these conditions were met.

4.0 ANALYSIS OF METEOROLOGICAL CONDITIONS FOR OWWE

In this section we examine the meteorological conditions for three cases flown during OWWE where N42RF experienced high winds at low altitudes. These are (a) the flight in question late on February 9, 2007; (b) the previous day's flight in a similar extra-tropical cyclone, February 8, 2007; and (c) a large frontal feature on January 22, 2007. Because of the similarities of the February cases, analysis will focus around a compare/contrast study between these two events. It is hoped that by doing such an analysis, better guidance can be developed to avoid future incidents.

Analyses center on a number products generated at NRL:

- a) Navy Coupled Ocean/Atmosphere Mesoscale Prediction System–On Scene (COAMPS-OS^{®*}): The bulk of our analysis is based on COAMPS-OS[®] model output. COAMPS-OS[®] is a turnkey mesoscale model built around the research and operation version 3.0 of COAMPS[®], operationally run at the U.S. Navy's Fleet Numerical Meteorology and Oceanography Center (FNMOC), and used by NRL scientists for basic research. COAMPS[®] is non-hydrostatic, compressible, and includes explicit cloud microphysics [Hodur 1997]. For this study, COAMPS-OS[®] was run from 00 Z February 6 through 12 Z February 11. Model boundary conditions were provided from 1 degree NOGAPS fields (see below). Mesoscale data assimilation is performed at 12-hour incremental update cycles also using NOGAPS data fields. Simulations occurred in two grid domains. The 121×91 outer grid was set to 54 km resolution and spanned a range from the eastern United States to western Europe (see Figure 6 for outer grid coverage). A 121×91 pixel 18 km inner grid was used to model the range of most intense cyclogenesis and centered at 45 W, 45 N. During the event of February 9, automated confidence levels for temperature and dew point were within a few degrees Celsius. Relative humidity was considered better than $\pm 20\%$ over the region. Wind speed errors were on the order of 5 to 10 kts, or $<15\%$ of winds in the operations area, with wind direction being better than 10 degrees.

* COAMPS[®] and COAMPS-OS[®] are registered trademarks of the Naval Research Laboratory

- b) Navy Operational Global Atmospheric Prediction System (NOGAPS): NOGAPS, developed at the Naval Research Laboratory, is the U.S. Navy's operational global numerical weather prediction model, providing products and guidance for the Department of Defense (*Hogan and Rosmond* 1991). Run operationally at 0.5×0.5 degrees and 27 levels, products are averaged to 1×1 for use in other models or as overlays on satellite products such as Figures 1 and 2. NOGAPS products can be found at <https://www.fnmoc.navy.mil/PUBLIC/>.
- c) Remote Sensing Products: The Remote Sensing Section of the Naval Research Laboratory's Marine Meteorology Division generates over 90,000 images and products daily. Because these research flights are mostly conducted at night, infrared imagery from Meteosat-8/SEVERI were heavily utilized. Also generated are fused TRMM/SSMI/Geostationary precipitation products [*Turk and Miller* 2005] as well as CloudSat space-based radar profiles. Because TRMM does not reach these high latitudes, the analysis is more heavily dependent on a regression of SSMI microwave data onto geostationary based features. While less accurate than the more active methods such as TRMM, the geostationary contribution typically places precipitation features well qualitatively. An excellent starting point for exploring available satellite products can be found at http://www.nrlmry.navy.mil/sat_products.html.
- d) NRL Aerosol Analysis and Prediction System (NAAPS): Running at FNMOC in the last year, NAAPS is the world's first and still only truly operational global aerosol model. NAAPS is an offline model that uses NOGAPS wind and state variable output to generate, transport, and scavenge aerosol particles. Currently, sulfate, dust, and smoke components are running operationally. Recently, a sea salt parameterization has been developed and is run in beta testing mode at NRL [*Witek et al.* 2007]. NAAPS products can be found at <http://www.nrlmry.navy.mil/aerosol/>.
- e) N42RF flight data: Data collected during OWWE were invaluable in this analysis. Most of our analysis of collected data centers on a series of dropsondes released throughout the mission. Also, state and wind data collected directly on the aircraft provided valuable indicators of the conditions leading to the event.

4.1 Model Results for the February 8 and 9 Events

On February 8 and 9, N42RF performed research flights in a pair of explosive cyclogenesis events which rapidly developed ~10 degrees due east of Maine and Newfoundland. COAMPS-OS[®] 54 km outer grid 700 mb geopotential heights are presented in Figure 6, showing the spawning of these storms from 12 Z on February 8 through the time of the incident at 21 Z on February 9. The most dominant feature is a deep cutoff low that persisted for the entire first third of the month of February. The associated surface low center migrated in the region between northern Newfoundland and southern Greenland, with central pressures ranging from 969 to 990 mb. Throughout its existence, a series of short waves rotated through this large mid-level feature. Upon leaving the North American continent, these short waves rapidly developed into extra-tropical cyclones, with maximum deepening occurring once they reached the Gulf Stream. In fact, the relative position of this larger parent low relative to the Gulf Stream allowed the shortwaves to propagate right up the tongue of warm water enabling the rapid intensification of each surface low. By late February 9, the anchor low began to fill and a building ridge over the Hudson Bay blocked further short wave propagation into the North Atlantic.

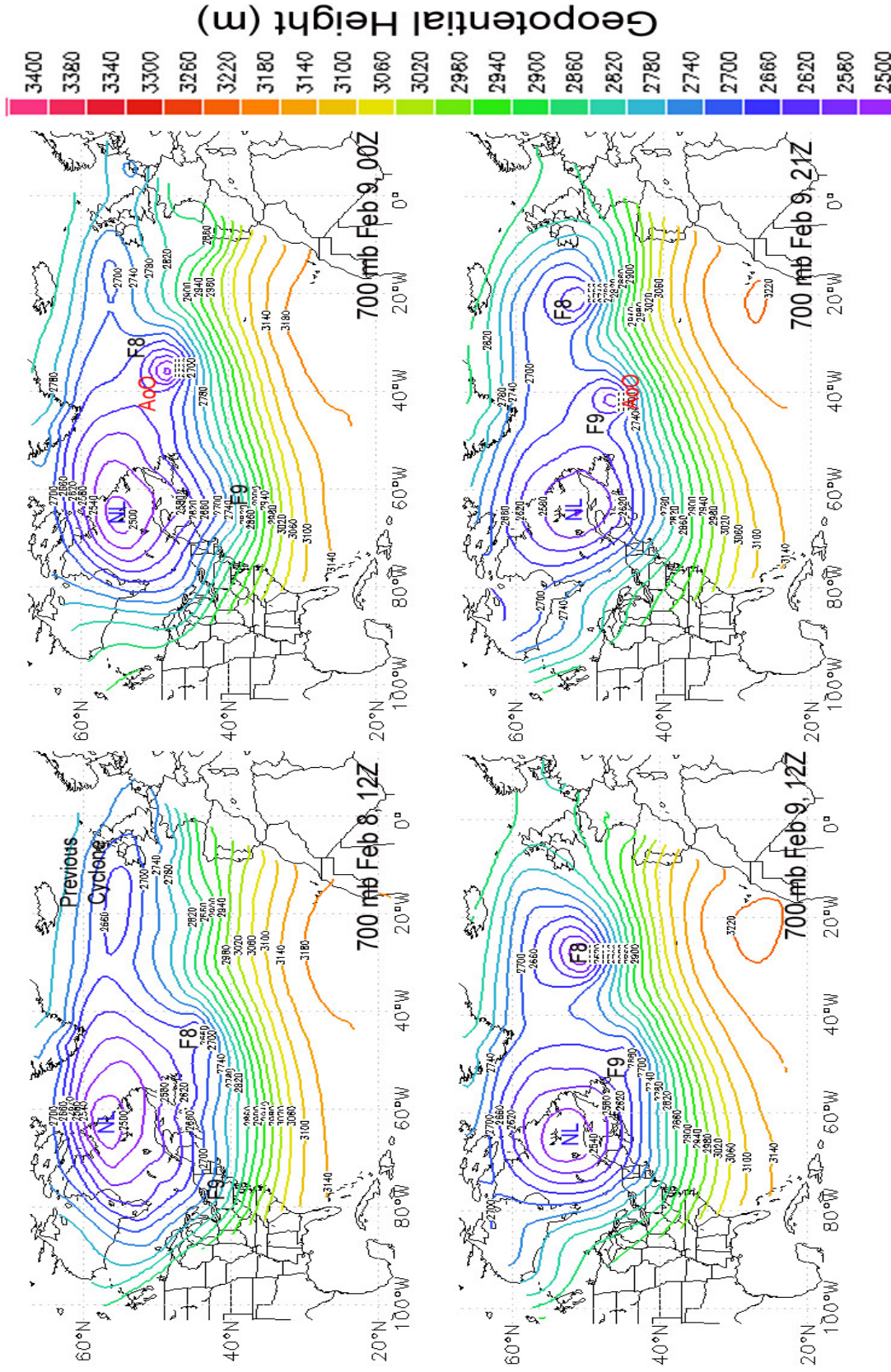


Figure 6. COAMPS® -OS outer grid 700 mb geopotential height fields for February 8–9, 2007. Marked are the parent Newfoundland Low (NL), the storm sampled on February 8 (F8), and the storm of the day of the engine stall incident, February 9 (F9). Also marked are the N42RF Areas of Operation (AoO) for the two flights described here.

Labels of the two extra-tropical cyclones sampled by N42RF for February 8 and 9 are included in Figure 6, as is the parent Newfoundland low (henceforth NL). The two extra-tropical cyclones modeled for this study fit the classic definition of explosive cyclogenesis where their central lows deepened by more than 24 mb in 24 hours. At the time of the F8 and F9 flights, COAMPS-OS[®] modeled surface pressure for F8 and F9 for the previous 24 hours deepened from 993 to 960 mb and 993 to 968 mb, respectively. Both flights appear to have occurred during mature phases of the storms and during maximum wind speeds. After sampling, the storms weakened, and propagated into Ireland and northern France.

To understand the circumstances leading to the events on February 9, it helps to briefly review the structure of powerful Atlantic cyclones. Figure 7 presents a Meteosat-8/SEVERI IR image for 21:00 Z on February 9 (city lights, in yellow, are from a static DMSM background image). Overlaid is the NOGAPS 500 mb geopotential height field. Basic structure is not conceptually unlike the classic Norwegian model of a mature extra-tropical cyclone. For the F9 case, a cold front is located behind the warm conveyor, identifiable by the long cloud formation. A weak warm front is also discernible. The F9 event is clearly in a mature stage with a characteristic “comma cloud” pattern indicative of a bent-back warm-type occluded front and frontal t-bone [Shapiro and Keyser 1990]. At this stage of a mature marine cyclone, hurricane force winds are common in the cold air side of the cold front and the elongated westerly flow creates especially long fetch regions. Also visible is the cyclone sampled 21 hours earlier (F8), which is now rapidly weakening.

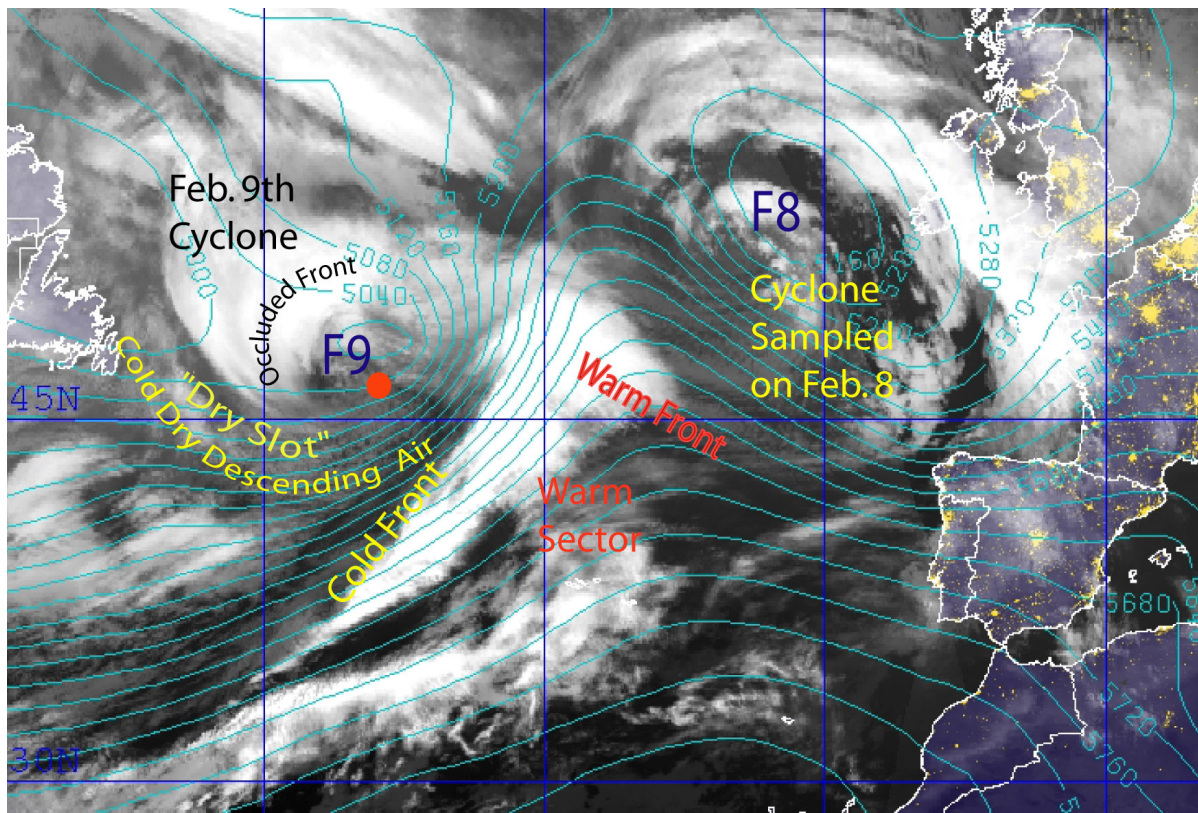


Figure 7. Meteosat-8/SEVERI image for 21 Z on February 9, 2007, of the extra-tropical cyclones sampled on February 8 and 9. Overlaid are NOGAPS 500 mb geopotential heights as well as annotations of key features. Marked in red is the point where N42RF shut down its engines.

The most important feature discernable for this analysis from Figure 7 is the slot of cold and dry descending air behind the occluded front. This feature is commonly referred to as the “dry slot” or “cold tongue” of a storm. While the cold air advection over the warmer ocean promotes mixing and convection, the very low humidity and adiabatic subsidence warming aloft of this air-mass inhibits cloud formation and consequently precipitation. In fact, in this particular case this polar air mass has proceeded so far into the storm that its impact can be seen in suppressed cloud cover in the “notch” region between the cold front and the occluded front.

Based on the COAMPS-OS[®] model run for this analysis plus the conceptual model presented above, we can do a compare and contrast study of the F8 and F9 events. These can be seen in the COAMPS[®] inner-mesh field presented in Figures 8, 9, and 10, where surface, 1000 m (i.e., flight level) and 2000 m (i.e., COAMPS[®] inner simulated cloud bases and boundary layer height) wind and temperature data are given. For surface data, modeled sea surface temperatures are also given. Figure 11 presents the NRL satellite-based precipitation product.

Structurally the F8 and F9 storms are fairly similar. Both are true explosive cyclogenesis events that followed similar tracks up the Gulf Stream. Both had observed peak surface wind speeds over 90+ kts (45 m s^{-1} , equivalent Saffir-Simpson Category 2 hurricane wind speeds). Air temperatures are alike. Wave Watch 3 (WW3) model runs (not shown) also had similar wave features, with maximum significant wave heights at 10–15 m. Both storms followed similar tracks up the Gulf Stream. The distribution of SST and air temperature indicates that, in general, air-sea temperature differences for the two storms are also fairly similar.

On cursory inspection of model output there are a few differences. Of the pair, F8 was definitely more powerful, with a deeper modeled low than F9 (952 mb versus 968 mb, respectively). Surface wind speeds were also slightly higher for F8 than for F9. Apparent from the COAMPS-OS[®] simulation is that while F9 was nearing maximum development during the flight, F8 was just beginning to decay, with maximum modeled wind features (100+ kts) and surface pressure of 952 mb reached approximately 2 hours earlier at 22:00 Z (22:00 Z is within the F8 flight but did not correspond to maximum storm penetration at ~00 Z on February 9). This is supported by the further and more developed propagation of cold air around the low into the occluded front.

Despite having a less intense surface pressure minimum, F9 demonstrated a more extensive 2000 m wind field (see Figure 10). However, this did not manifest itself in significantly higher wind speeds at the surface (perhaps ~5 kts or 2 m s^{-1} , see Figure 8). This suggests lower boundary layer heights for F9 as surface drag is not interacting with winds aloft. Indeed, modeled boundary layer heights for F8 were also slightly higher, on the order of 1800–2000 m, compared to 1500–1800 m for F9.

Lastly, we considered both modeled and satellite-derived precipitation. Again, as expected, these two systems are similar, with precipitation occurring along the cold front and through the occluded front, with minimal precipitation in the cold descending air. Both model results and satellite retrievals have higher precipitation in F8 relative to F9, although the satellite product does place some scattered precipitation in the cold air-mass south of the low.

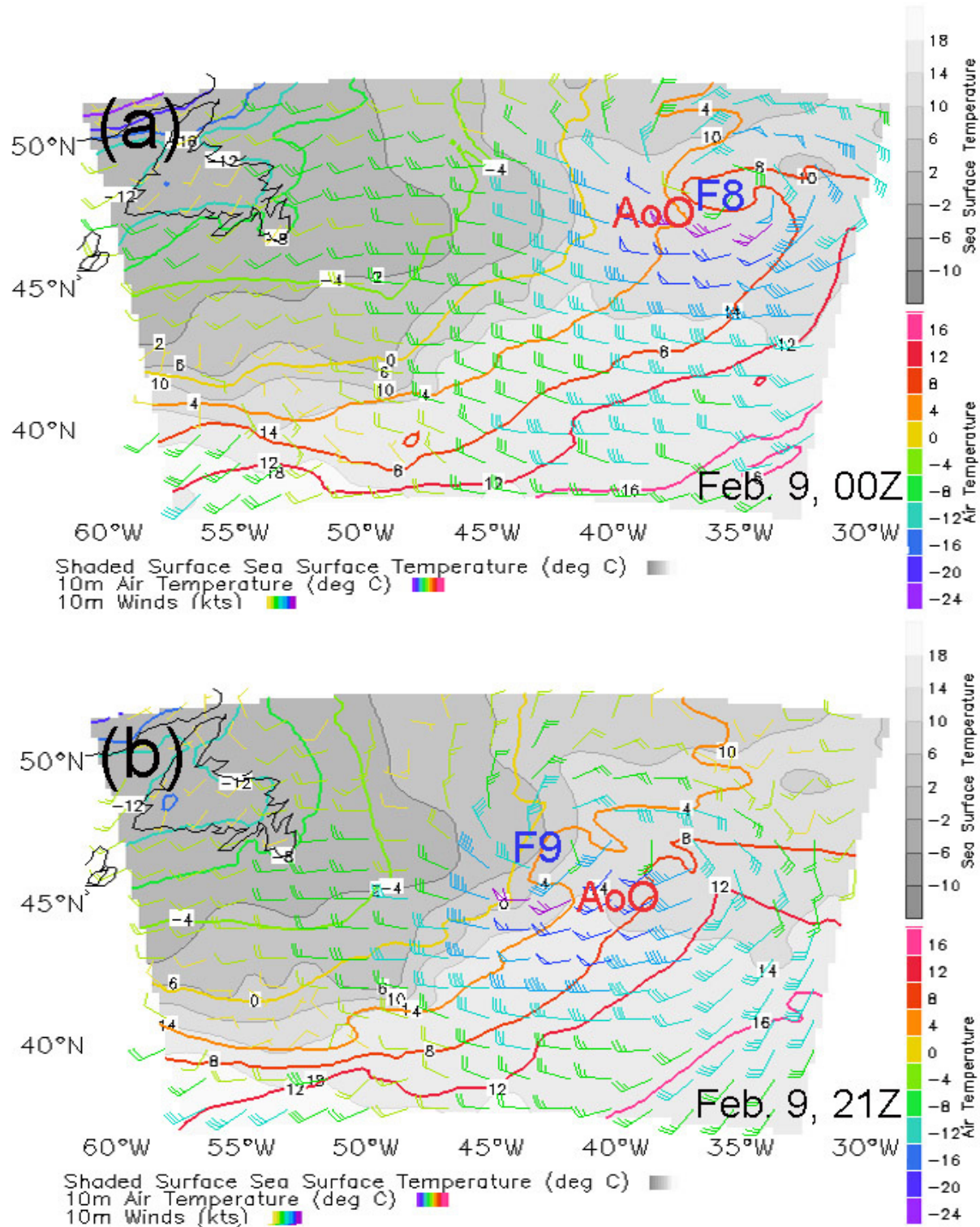


Figure 8. COAMPS[®] inner grid (18 km) 10 m air temperature (°C), 10 m winds (kts), and sea surface temperature (°C), for (a) February 9, 00 Z and (b) February 9, 21 Z. Also marked are the N42RF Areas of Operation (AoO) and the low centers (F8 and F9).

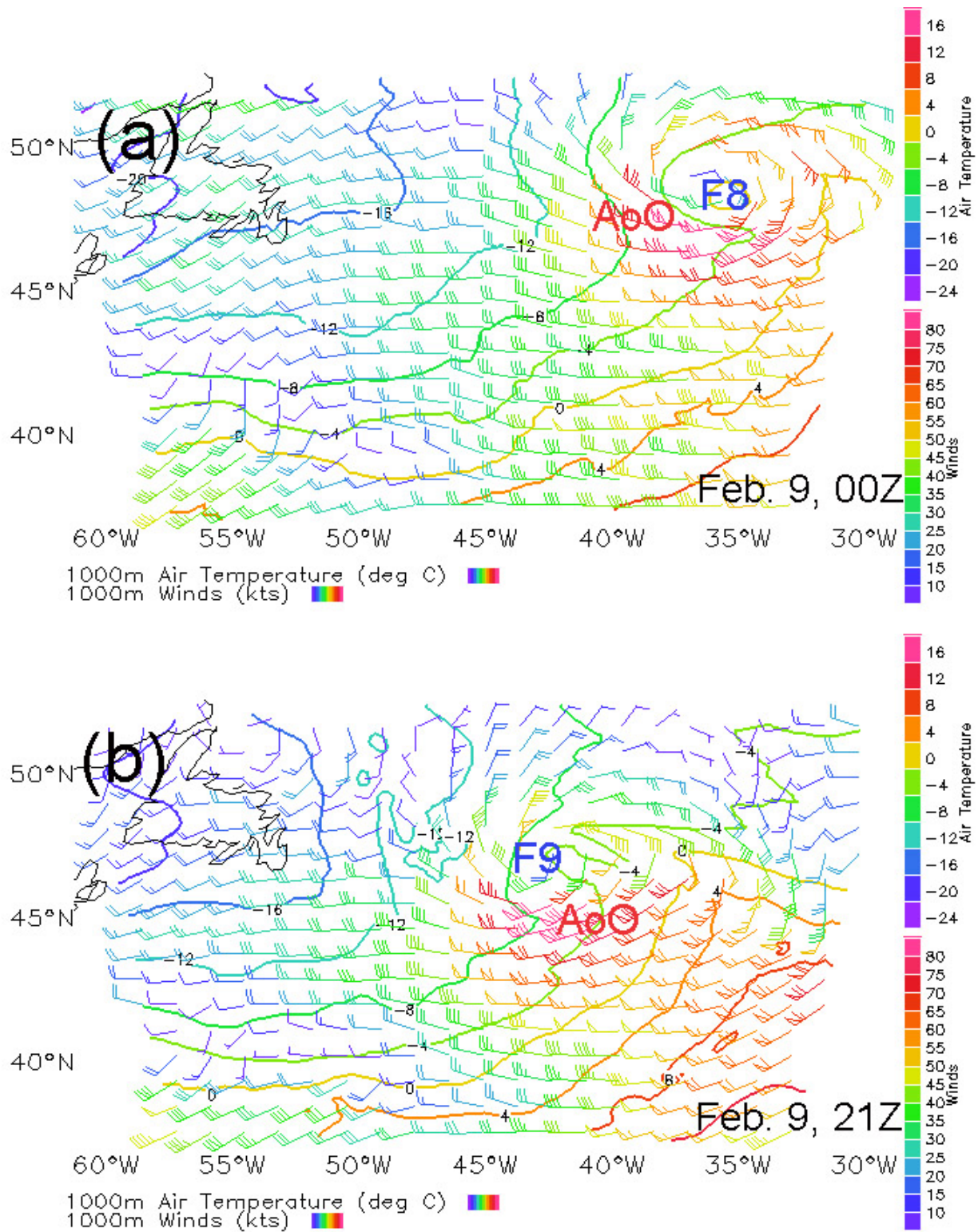


Figure 9. COAMPS[®] inner grid (18 km) flight level (1000 m) air temperature (°C) and winds (kts), for (a) February 9, 00 Z and (b) February 9, 21 Z. Also marked are the N42RF Areas of Operation (AoO) and the low centers (F8 and F9).

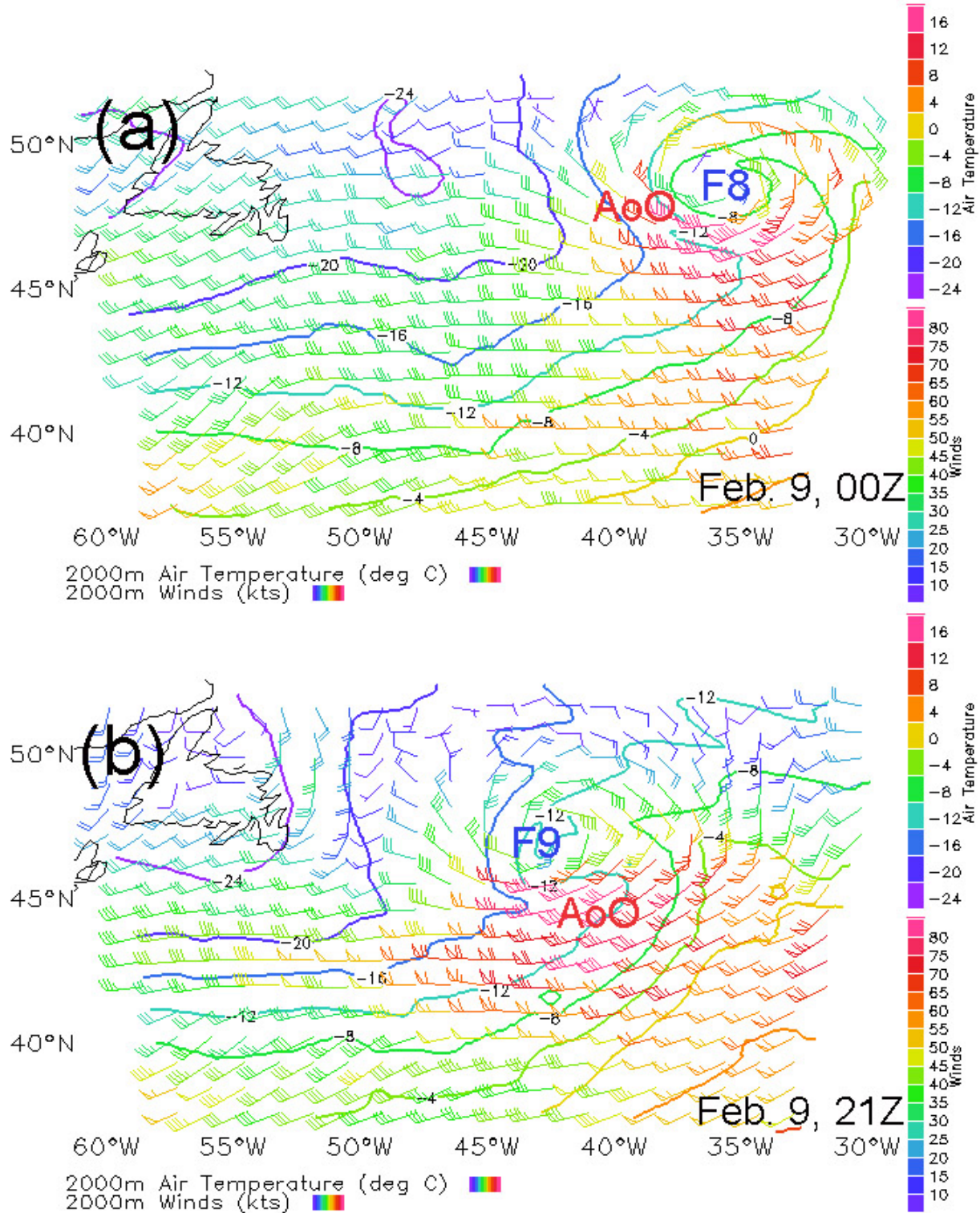


Figure 10. COAMPS[®] inner grid (18 km) 2000 m air temperature (°C) and winds (kts), for (a) February 9, 00 Z and (b) February 9, 21 Z. Also marked are the N42RF Areas of Operation (AoO) and the low centers (F8 and F9).

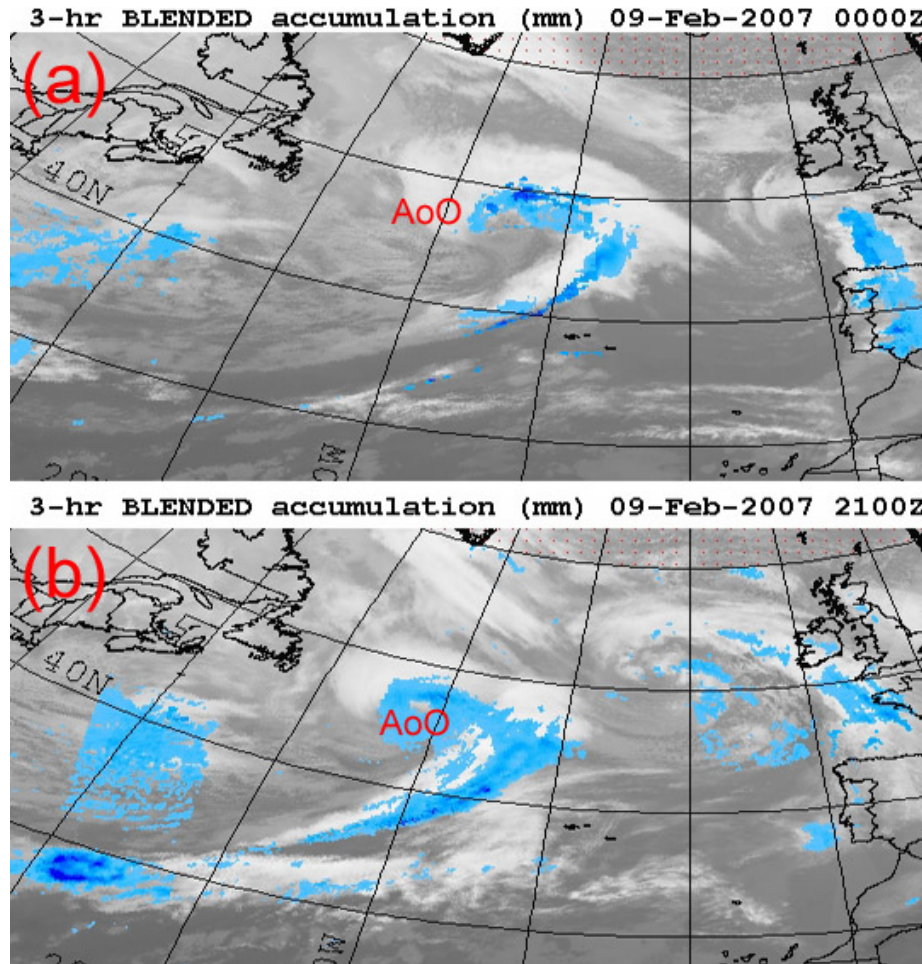


Figure 11. Blended NRL SSMI/geostationary precipitation product for the flights of Feb. 8 and Feb. 9 in (a) and (b), respectively. At these latitudes, this precipitation product should be treated as qualitative. Overlaid is the general aircraft Area of Operation (AoO).

Based on the conceptual model of these systems and the above analysis, the situation regarding the extreme sea salt conditions experienced by N42RF is quite clear. The MBL region with the highest burden of sea salt is in the dry slot of cold and dry descending air wrapping around the occluded front. Not only does this air have the highest wind speeds, but south to southeast of the low it can have extremely large fetches, on the order of 300–500 km. This region also exhibits the highest significant wave heights for a storm as well. This leads to increased momentum flux to the surface and presumably higher aerosolization of sea water. Cold air advection over the Gulf Stream increases boundary layer instability at the surface allowing large sea salt particles to be vertically mixed. However, the descending motion of the air aloft caps convection and inhibits precipitation. Consequently, sea salt concentrations can maximize in this region.

The F9 flight focused south-southeast of the low. Indeed, as is seen in Figures 1 and 7, N42RF's flight path maximized its exposure in this high sea salt environment. Conversely, for the F8 storm, despite the high wind speeds experienced by N42RF, the aircraft did not fully penetrate the occluded front (Figure 2). Hence, for F8, N42RF sampled air with lower wind fetch, higher stability, and

adjacent to precipitation zones. Had N42RF flown a similar storm-relative path for F8, similar high sea salt concentrations would likely have been experienced.

4.2 Meteorological Data for February 8 and 9

While the model data and analysis in Section 4.1 provides a working conceptual model, we also have the benefit of data collected on N42RF to corroborate our analysis and conclusions. Not only can this data fine-tune the modeling results, but it can also lead to potential indicators that can help flight meteorologists identify this type of situation. An important first point is that events leading to sea salt induced engine loss cannot be simply related to wind speed. Anecdotally, this is well realized by the thousands of problem-free hours flown by NOAA WP-3 aircraft; only on two occasions (this and CBLAST) has there been engine disruption due to sea salt. As is demonstrated in the flight data, a number of key elements were required in order for the hazardous concentrations of sea salt to exist.

Figure 12(a) presents flight level wind. For the flight on F8, wind speed and direction traces presented are consistent with the satellite and NOGAPS overlay in Figure 2. At flight level (~850–900 m), winds remained westerly around the occluded front identifiable by the high winds, peaking at 100 kts (50 m s^{-1}). Dropsondes released in the first penetration (eastern peak on the plot) suggested 65 kts (32 m s^{-1}) winds at the surface, and highly unstable lapse rates of $10\text{--}11 \text{ }^\circ\text{C km}^{-1}$ through the MBL and up to $16 \text{ }^\circ\text{C km}^{-1}$ for the lowest hundred meters. 925 mb (~450 m) temperatures were cold, on the order of 0° to $-3 \text{ }^\circ\text{C}$ (925 mb is used a good indicator of MBL temperature, because it is not too close to the surface where sensible heat flux would dominate the reading). In one instance the MBL was saturated. Upon penetrating the occluded front, wind speeds dropped precipitously and direction shifted to west-southwest. This is because the aircraft was essentially in the middle of the low. For the return leg to the airfield (more westward peak in wind speed) the same pattern is observable.

Nominally these conditions meet some hypothesized minimum requirements for extreme sea salt events. High winds coupled with instability should result in large atmospheric burdens of sea salt particles. However, there are several key requirements that are not met. Most importantly, while wind speeds are high, upwind precipitation-free fetch is low (<100 km at maximum). This fetch issue manifests itself in several ways. First, the atmosphere can require several hours to reach equilibrium with regards to production and deposition of sea salt. Any instance of precipitation will rapidly scavenge sea salt from the MBL and restart the processes. Second (and perhaps even more important in this case), increased wind fetch also results in more active sea states. In the region of high winds around the F8 occluded front, the Wave Watch 3 model has significant wave heights on the order of 3–6 m, less than half that in the cold air tongue southeast of the low. Lastly, the moment winds subside (say near the border of the occluded front), any giant mode sea salt generated in the high wind regions and advected into the low would rapidly fall out.

Now consider the F9 flight (Figure 12(b)), also at ~850–950 m altitude. Wind traces show a similar pattern through the wall of the occluded front (-45 to -43 longitude) and transit across the inner low (-43 to -42 longitude). Around the occluded front, winds are high (up to 80 kts, 40 m s^{-1} , at flight level) but not quite as high as the F8 case. However, as the aircraft passed through the low into the high wind/cold tongue region to the southeast, winds shift to the west-southwest and rapidly increase to an average of 90 ± 5 kts at flight level. Dropsondes indicated 10 m winds at $\sim 35 \text{ m s}^{-1}$ and again unstable conditions $10\text{--}11 \text{ }^\circ\text{C km}^{-1}$. (These winds are slightly higher than those in the COAMPS-OS[®] simulations, which suggested ~85 and 60 kts at 1000 m and 10 m, respectively.) The last dropsonde released a few minutes before the first engine fire report measured surface winds at 41 m s^{-1} . 925 mb temperatures averaged $0 \text{ }^\circ\text{C}$, or potential temperature of $\sim 4.5 \text{ }^\circ\text{C}$, or roughly $10 \text{ }^\circ\text{C}$ cooler than the ocean surface temperature of $\sim 14 \text{ }^\circ\text{C}$. No data were collected on the return leg of this flight.

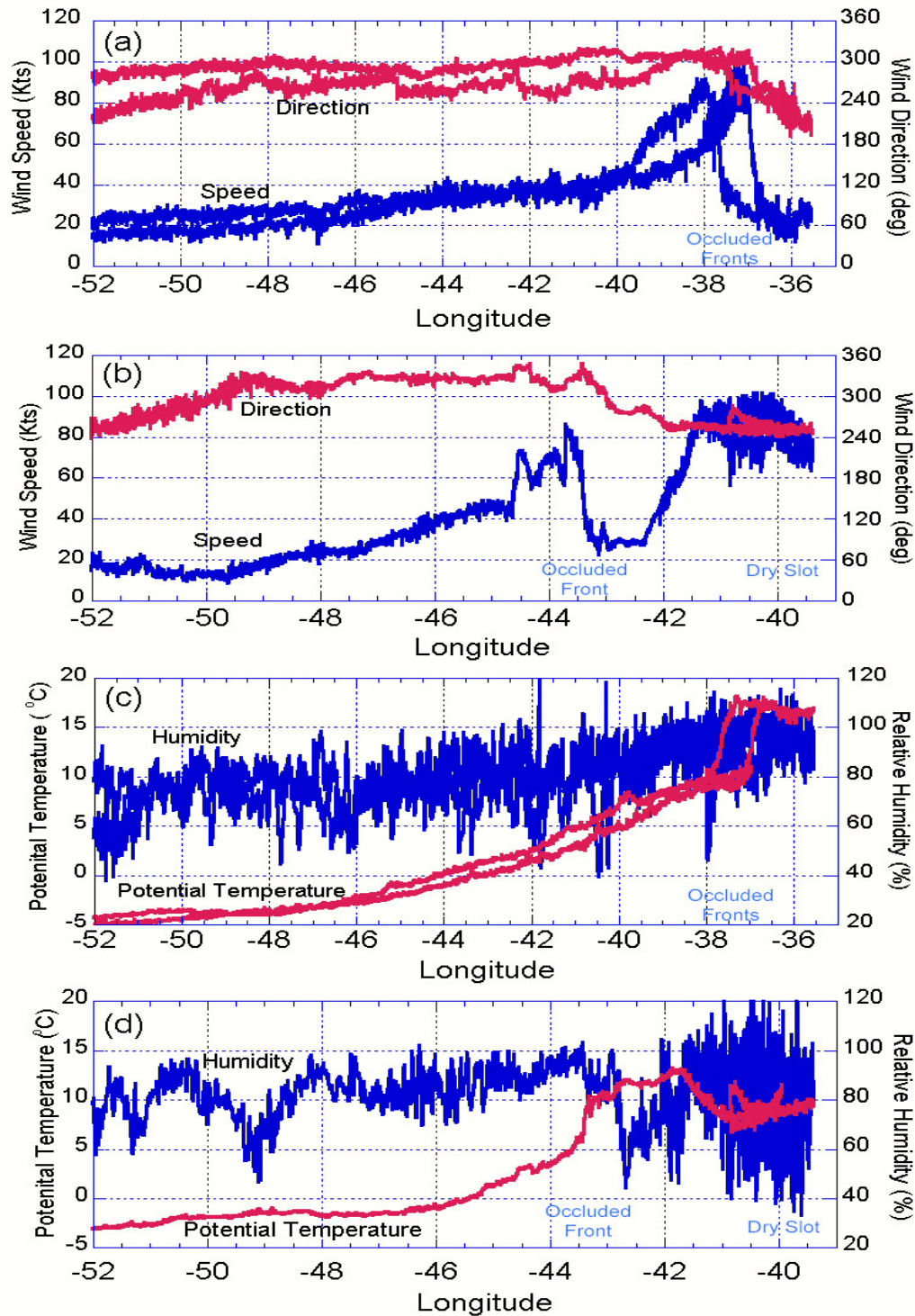


Figure 12. Longitudinal dependence of wind, potential temperature, and humidity along the flight tracks for (a) and (c), the February 8 flight, and (b) and (d), the February 9 flight. Note the dramatic increase in dew point and wind variability at ~ 41.5 W in (b) and (d) as the aircraft flew into the highly unstable dry slot southeast of the occluded front.

For the F9 case again, measured winds and instability are similar to F8. But the most significant difference is that in the F9 flight region the sampled air-mass had over 400 km of precipitation-free fetch. Not only did this increase the particle concentration, but also allowed a significant surface wave field to develop, with WW3 significant wave heights at 10–15 m.

A second point of difference between the F8 and F9 may be due to the amount of mixing turbulence and humidity variability in the marine boundary layer. As stated above, dropsonde lapse rates were fairly similar for the two flights, thus giving the impression of similar mixing. However, it is very difficult for the atmosphere to sustain super-adiabatic lapse rates except very near the source region, in this case the surface. Even the observed MBL average lapse rates of 10° to $11^{\circ} \text{C km}^{-1}$ (compared to the standard adiabatic $9.8^{\circ} \text{C km}^{-1}$) are fairly extreme in the authors' own experience. Given the situation, a secondary indicator of mixing would be helpful.

NOAA flight meteorologists pointed out in their analysis that one notable difference between F8 and F9 was that just before the engine fire on F9, humidity readings began oscillating dramatically. This is demonstrated in Figure 12(c) and (d) where potential temperature and relative humidity traces for the F8 and F9 flights are presented, respectively. The location occluded frontal zone is clearly visible in these traces with rapid increases in temperature, followed by a subsequent drop in the dry slot to the east. For the F8 flight, there is a fair amount of variability in the relative humidity trace, on the order of $\pm 10\%$ RH (RH values are calculated and data presented above 100% are due to response differences between temperature and dew point probes). Because the F8 storm had moved far into the Atlantic, such variability is not unexpected. The flight track had N42RF transiting long distances in the cold polar air over the warm Gulf Stream waters. Thus, this variability is a result of the aircraft flying through large eddies in the atmosphere, as the heat flux at the surface warms and moistens the lower boundary layer and is exchanged with the cold dry air above. Because this is mostly at low wind speeds, sea salt production is low and consequently so is the concentration of particles at flight level. Once N42RF reached the occluded front, air temperatures were higher, the atmosphere moister, and ultimately stability was increased.

In the case of the F9 flight, patterns are again similar up through the occluded front, including the dampening of the RH variability around the occluded front itself. However, as N42RF transited into the high wind region southeast of the low (-41.5 longitude), we find large oscillations in the RH series. Within minute time frames, recorded RH at flight level ranged from 40 to 100%, coinciding with estimated updraft velocities of nearly 5 m s^{-1} . Coincidentally, pilots reported at this time obscured visibility on the cockpit windscreen due to sea salt. This is a clear indication that at this point the aircraft began to collect salt on the airframe and engines in significant quantities.

Originally, NOAA staff meteorologists hypothesized that this extreme variability (unseen before in their personal experiences) may have been due to sea salt contamination on the aircraft's chilled mirror dew point hygrometer from which the RH value is derived. To test this hypothesis, we compared the chilled mirror system to a rapid-response secondary tunable diode laser (TDL) hygrometer also onboard. A sample time series and scatter plot extracted in a severe period of instability is presented in Figure 13. Correlations are excellent and point against contamination (offsets for IR systems like the TDL are not uncommon). Scatter that does exist is most likely due to the differences between the relatively fast (10 Hz) TDL and slow (>5 second, with internal oscillations) chilled mirror instruments. Thus, these oscillations are in fact due to the aircraft intersecting coherent ejection eddies of moist air from below.

This variability in humidity experienced by the WP-3D for the F9 flight may also have additional implications for sea salt fouling. Sea salt is typically considered "hydrated" in the MBL, owing to it always being produced "wet," and relative humidity is typically on the order of 60–100%. These values are well above the efflorescence humidity at $\sim 35\text{--}40\%$. At 80% RH, the hygroscopicity curves

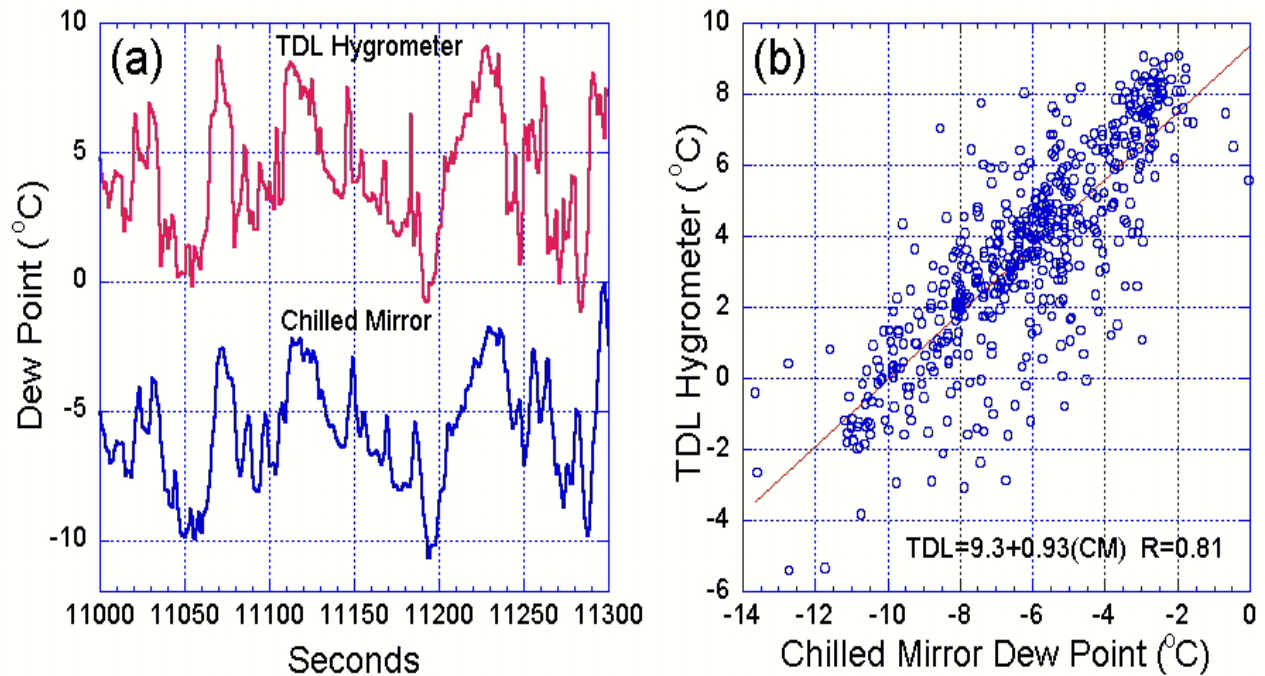


Figure 13. Five minute data selection of N42RF's chilled mirror and tunable diode laser (TDL) hygrometer while the aircraft was likely in heavy sea salt concentrations (start: 21:26:00 UTC). (a) 1 Hz time series comparison. (b) Scatter plot of data in (a).

suggest that a sea salt aerosol particle will be 90% water. Thus, we would not expect sea salt to necessarily dramatically accumulate. But if the RH drops to around 40%, significant drying and crystallization may occur.

Typically, air-sea exchange is characterized by long gradual increases in humidity and temperature (an ejection), followed by a dramatic drop associated with a turbulent eddy from above (or a sweep). At the top of the boundary layer, the opposite is true, where long periods of down-welling air masses are punctuated by individual convective updrafts. This is visible if one plots the distribution of aircraft-measured vertical velocity where a definite skewness is evident in the vertical velocity histogram. Since the WP-3D was intersecting warm, moist, and sea salt laden updrafts in between longer periods of drier environments, it is possible that increased sea salt accretion developed through the oscillating wet-dry cycle.

4.3 Estimates of Boundary Layer Height

As discussed in Section 4.1, COAMPS-OS[®] simulations of the F8 and F9 storms placed the boundary layer at ~1800–2000 m and 1500–1800 m, respectively. However, boundary layer parameterizations are not well tested, and even the definition of boundary layer in these conditions has some ambiguity. Because the OWWE flight plan kept N42RF to altitudes below 1000 m, there is no direct data of marine layer heights along the flight track. Nor are there readily available findings in the peer-reviewed literature. Thus, with the analysis up to this point, we are not in a position to answer the key question of what altitude N42RF needed to fly at to stay clear of giant sea salt particles.

In the summer of 2006, NASA launched the Cloud-Aerosol Lidar and Infrared Pathfinder Satellite Observation (CALIPSO) satellite. The CALIPSO instrument includes 532 and 1064 nm lidar systems

for making high vertical resolution measurements of aerosol and thin cloud structure. CALIPSO tracks serendipitously passed over the F8 and F9 storms, approximately 4 and 7 hours after the F8 and F9 research flights. While the timing is not optimal, CALIPSO does provide us with valuable structure information in the cold dry slots of these two storms. Figure 14 presents the CALIPSO 532 nm attenuated backscatter signal for the F8 and F9 storm systems. Also included are the lidar tracks over IR geostationary imagery. The CALIPSO track from north to south corresponds to left to right.

The lidar track for F8 passed just east of the storm center, just short of the cold front. Clearly visible is the occluded front, dry air slot, and tip of the cold front. Clouds from the occluded and cold fronts are so thick that the beam cannot penetrate. However, the structure of the dry slot is captured well. The lidar backscatter shows strong returns in the lowest 2.5 km, topped with rapid decrease to clean tropospheric levels.

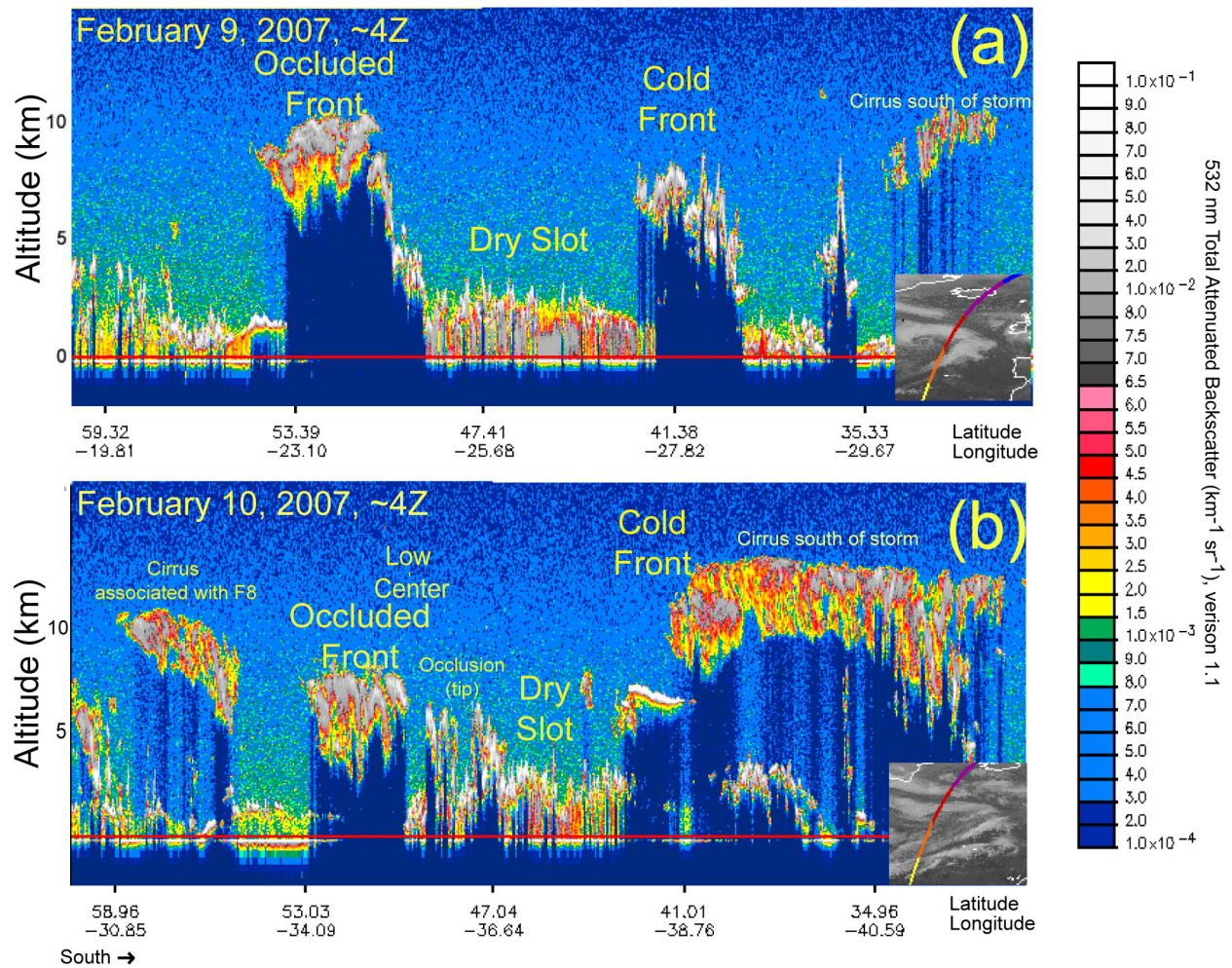


Figure 14. CALIPSO (version 1.1) 532 nm total attenuated backscatter ($\text{km}^{-1} \text{sr}^{-1}$) scans corresponding to the (a) February 8 and (b) February 9 storms. Included are corresponding Meteosat-8/SEVERI IR images with the orbit track overlaid. Image left to right corresponds to north to south. Imagery adapted from CALIPSO and CloudSAT websites: <http://www-calipso.larc.nasa.gov/products/lidar/>; <http://www.cloudsat.cira.colostate.edu/>

Within the MBL, the lidar return is not uniform but a secondary demarcation is visible at altitudes of 1.5–2.0 km. This is signified by a change in color from grey ($2.0 \times 10^{-2} \text{ km}^{-1} \text{ sr}^{-1}$) down to values nearly an order of magnitude lower in less than 300 m. Given the abrupt change in backscatter and uniformity to the surface, we surmise that this zone is the area of extreme sea salt. The gradient layer likely contains the true boundary layer transition where dry cold air aloft is exchanging with warm, moist, and sea salt particle laden air from below through both dry and (due to observed shallow cumulus in the region) moist processes. In the transition layer, updrafts are probably insufficient to keep giant particles aloft. The COAMPS[®] boundary layer height for along this track is 1500–1750 m, very close to our CALIPSO based estimate.

The F9 track is closer to the storm center and flight track than F8, but is structurally consistent with the F8 analysis with a clearly discernable dry slot. Since this track goes right over the low center, the occluded front “tip” can be viewed wrapping around the low. Height features in the dry slot are lower, with the transition zone between 1 and 2.0 km and the layer of well-mixed return at 1 to 1.2 km. This is not surprising, as F8 was a more powerful storm. Indeed, the COAMPS[®] boundary layer height for this track was globular in nature with 1000–2000 m heights, again very close to our CALIPSO based estimates.

Coincident with CALIPSO data collects is the CloudSat radar on the same platform (Figure 15). These cloud-penetrating 94-GHz radar profiles provide a more complete view of the storm and highlight large cloud droplets, ice, and precipitation. Within the dry slot, the radar profiles are consistent with the CALIPSO backscatter returns, indicating scattered cumulus with cloud tops coincident with top of the gradient zone but with isolated spikes that reach 3 km (~700 mb). These returns were strong enough to suggest that there may have been some minor precipitation associated with small clouds, which is consistent with the pilot debriefs. Because the data is preliminary, near the surface it would be difficult to quantitatively assess precipitation, or even differentiate precipitation from giant sea salt.

While CALIPSO and CloudSat give us detailed vertical profile information along very narrow tracks, extrapolation needs to be performed over the whole storm. Figure 16 presents MODIS imagery and level 2 products for the February 9 storm, with an overpass time of ~05 Z on February 10. Included are cloud top pressures, temperatures, and phases. Cloud features appear to be consistent across the dry slot (from behind the occluded front to the cold front), with cloud top heights varying from 800 mb from the smallest cumuli to some larger events reaching 700 mb (3 km). Cloud phase for these cumuli were typically ice, with some mixed phase tops—this is consistent with cloud top temperatures of -20°C . Based on the CloudSat returns, we should expect that these largest cells could form some light precipitation.

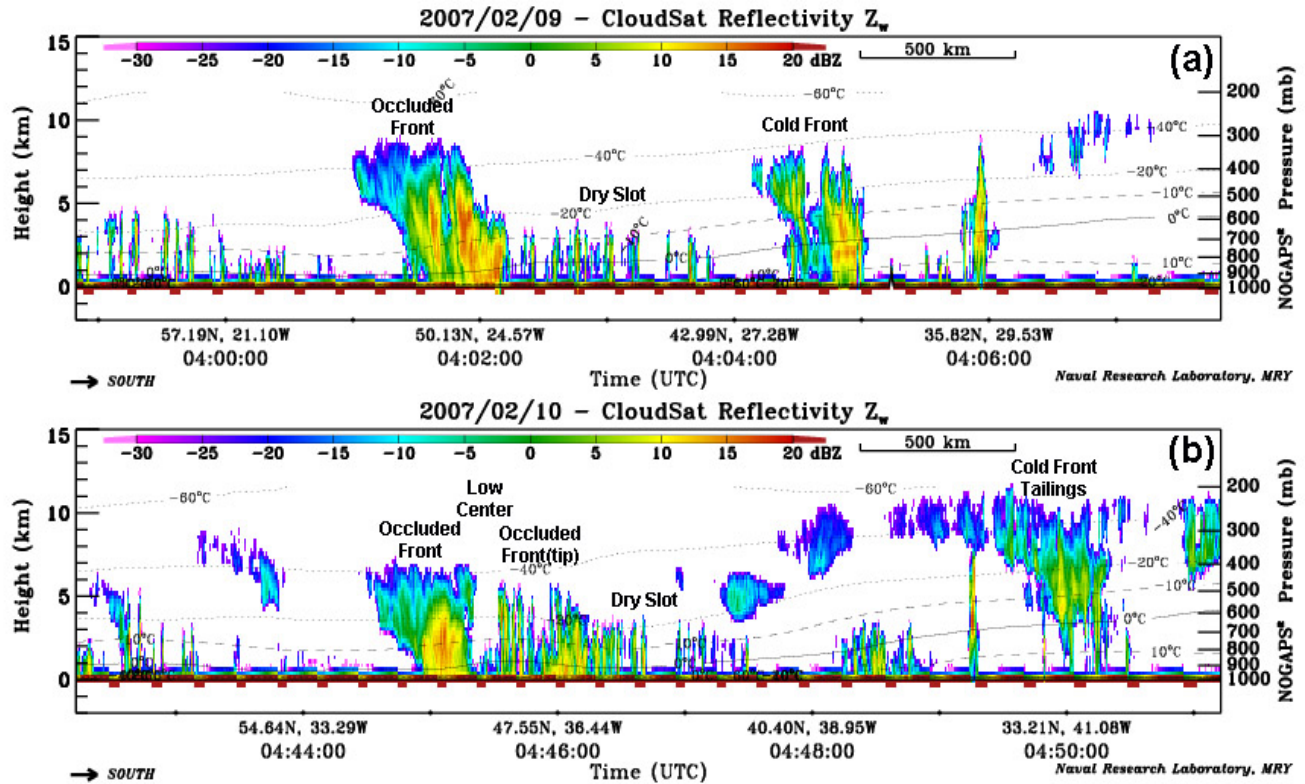


Figure 15. CloudSat 94-GHz reflectivity returns for the storms sampled on February 8 and 9. These scans correspond to the CALIPSO data presented in Figure 14. Imagery courtesy of Cristian Mitrescu (NRL).

4.4 The January 22 Case

We also performed a brief examination of the January 22 mission. While COAMPS-OS[®] simulations were not for J22, the nature of this event and why sea salt collection was not an issue is quite straightforward. In comparison to the F8 and F9 flights, the J22 OWWE flight is distinctly different. In this case, the storm was not an explosive cyclogenesis extra-tropical cyclone, but rather a deep trough moving over northern Atlantic waters. Figure 17 presents (a) a satellite image with 500 mb heights overlaid, and (b) the NRL satellite precipitation product. While the J22 flight did experience the highest winds of the OWWE mission at flight level over very long fetches (up to >100 kts for 600+ km), and was conducted over very high seas (WW3 indicated 10–15 m significant wave heights in the area of operation), surface winds were lower than both the F8 and F9 storms (~50 kts maximum dropsonde-measured surface winds). As discussed in Section 3, since it is assumed that salt flux goes as more than a cube power law with wind, this difference between the F8/F9 storm and J22 likely results in more than a factor of three in sea salt particle production.

Based on model and satellite data, the most defining feature of this storm is the widespread precipitation throughout the high wind area. This is confirmed by dropsondes where the MBL exhibited very moist boundary layers and moist adiabat lapse rates. Precipitation scavenging and near nucleation of airborne sea salt would certainly reduce salt concentrations.

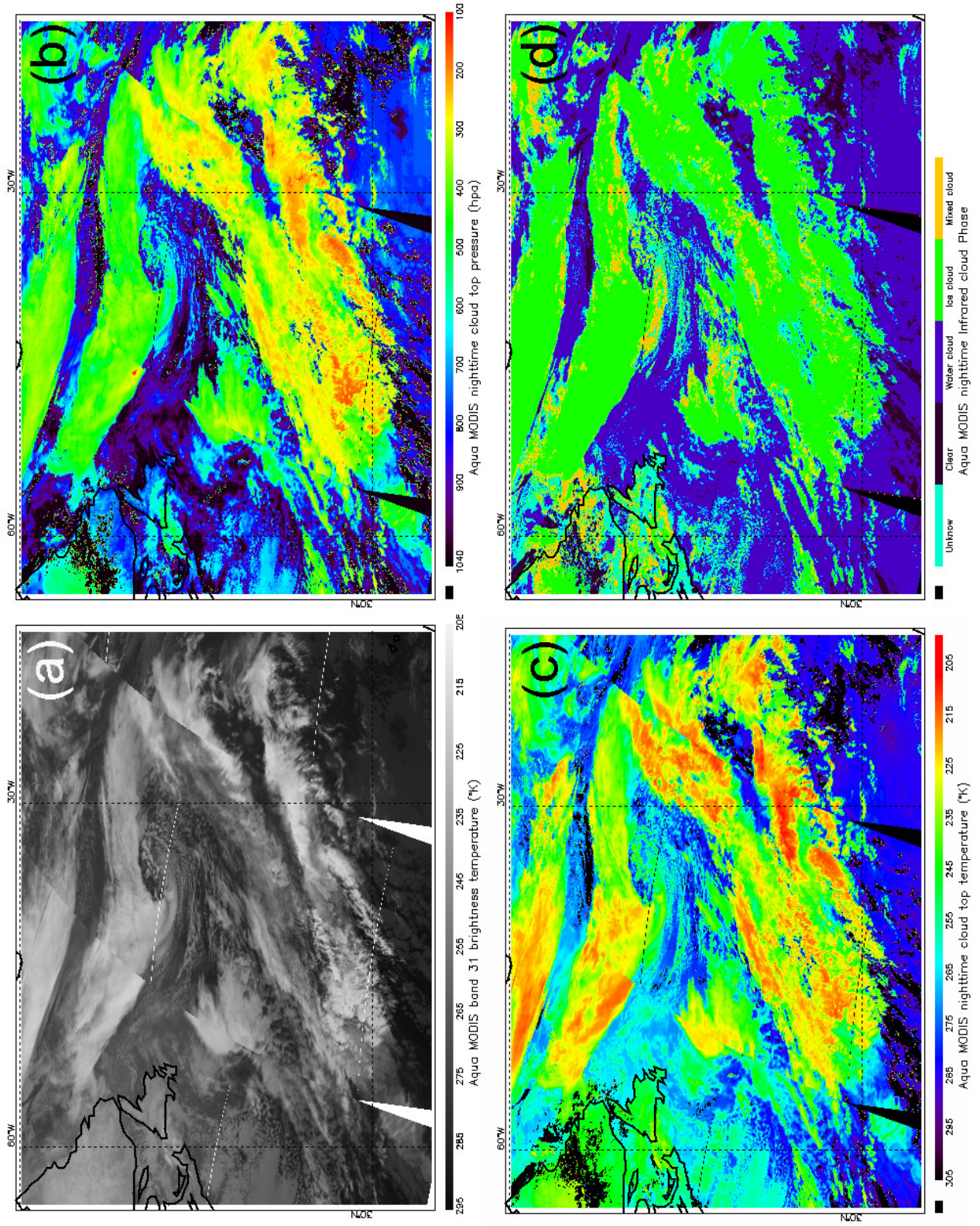


Figure 16. MODIS cloud products for the February 9, 2007, storm. Overpass time was ~05 Z on February 10.

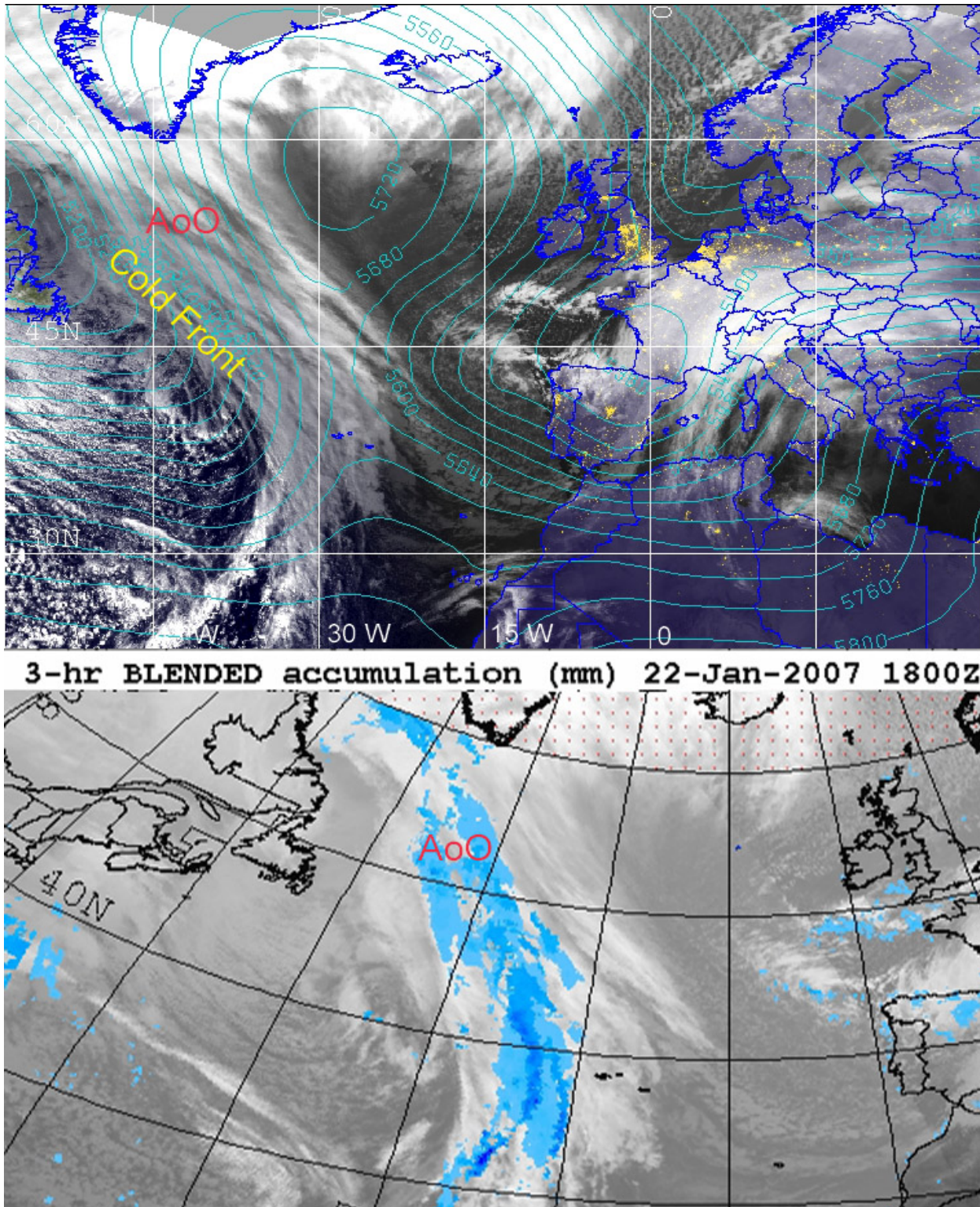


Figure 17. (a) Composite GOES/ Meteosast-8/SEVERI image for 18 Z January 22, 2007. Overlaid are NOGAPS 500 mb geopotential heights as well as annotations of key features. (b) 3-hour accumulation NRL precipitation product for the same time period. Areas of operation are marked by “AoO.”

5.0 SUMMARY METEOROLOGICAL GUIDANCE AND AVAILABLE PRODUCTS TO ASSESS SEA SALT CONDITIONS

The meteorological conditions experienced by N42RF on February 9 which led to multiple engine compressor stalls are unlike any other reported in the scientific community in severity and geographic extent. Even the engine compressor stalls reported on the sister WP-3D N43RF's following a low level (<400 m) CBLAST flight in dry slots of a hurricane were less intense than the event experienced here. Indeed, early discussions throughout the scientific community regarding the February 9 event resulted in some skepticism. However, with the benefit of post-flight analysis, we believe that we have presented a logical conceptual model that explains conditions of extreme atmospheric burdens of sea salt. However, it is emphasized that this analysis is based on one event; these conditions are still mostly unstudied, and many fundamental scientific questions remain unanswered. Indeed, this is a phenomenon never before considered by the atmospheric sciences community with potentially significant implications for sea salt aerosol-weather interactions. It is the intention of this report's authors to continue this research and develop more precise guidance.

5.1 Summary Meteorological Conditions

According to preliminary findings of the CBLAST program, high boundary layer winds coupled with unstable air can generate lower boundary layer ejection velocities well over 5 m s^{-1} , the velocity needed to suspend a $40 \text{ }\mu\text{m}$ sea salt particle. Even under more typical ocean conditions, we have found that $20 \text{ }\mu\text{m}$ sea salt particles are often well mixed in the marine boundary layer. Thus, prudence is warranted any time maritime flight operations occur in high wind conditions. Based on our literature review and on the conditions experienced during the February 9 flight, a preliminary caution threshold should be on the order of 30 m s^{-1} (~ 60 kts) for boundary layer flight (5 m s^{-1} or 10 kts less than that experienced on February 9). This number may need to be further reduced for lower boundary layer operations. Additional caution is warranted for higher surface wave heights. At higher significant wave heights, spume production is likely to increase. Again, based on this analysis $\sim 8 \text{ m}$ (25 ft) significant wave heights should be a baseline for potential hazardous sea salt concentrations for flight operations.

The most important consideration, however, is the distribution of precipitation. Precipitation is a very efficient scavenger of sea salt aerosol particles. Based on the incident report, engine cleansing via flight through less than 1 minute of precipitation may have contributed to the pilot's ability to restart engines. Clearly, boundary layer flight in regions with long, high wind fetches and low or scattered precipitation should be conducted under extreme caution. In the case of February 9, it appears that N42RF began accumulating sea salt in a region with 35 m s^{-1} surface winds, 400+ km of precipitation-free fetch, 15 m significant wave heights, and an unstable lapse rate.

While the lack of precipitation allowed for high sea salt concentrations in the atmosphere, what may have actually caused the severe accretion of sea salt on the aircraft was the particular moist-dry oscillation it encountered. As the aircraft flew in fairly dry descending air punctuated by severe moist aerosol-laden updrafts in the unstable dry slot, an accumulate-dry cycle formed thus leading to large crystal growth on the aircraft skin. However, such a process may not actually be relevant within the warm engine where drying would likely occur anyway. But this is an important hypothesis that should be considered by aircraft engineers.

5.2 Recommendations

The best defense for these situations is capable forecasters looking for the conditions listed above, taking into full account uncertainties and biases in models and satellite products. Explosive cyclogenesis events such as those sampled on February 8 and 9 are common, and the high wind and

dry, cold air slot that wraps around the low is a persistent feature for these storms. Similarities can be drawn to hurricanes and other high wind features.

During missions when caution is warranted, flight meteorologists should pay extra attention to available data sources. Dropsonde releases should be closely examined to help determine whether or not the aircraft actually is in the boundary layer—not always an easy interpretation flying at constant altitude within storms. Oscillations in vertical wind speed, temperature, and humidity proved also to be indicators of the salt fouling event. Additionally, close attention to storm relative position would be a powerful tool, especially if updated geostationary satellite images are available onboard. Commercial open-celled aerosol instruments are available that can measure giant airborne particles. While definitely beneficial, caution is warranted on depending on their regular application. These instruments do not have linear responses and a trained operator is needed to interpret the results. It is also possible that the salt fouling conditions experienced would also foul the optics of such devices. A discussion on the use of wing-mounted probes for studying sea salt can be found in *Reid et al.* [2006].

The sea salt accumulation on the cockpit windscreen was a leading indicator of this event. If aerosol probes or other in situ indicators are not going to become common equipment then the only mitigation is pilot recognition of the leading/lagging indicators and conditions where hazardous sea salt loadings occur.

While the evidence suggests that the engine fires were a result of a specific salt event, there is the possibility that salt accumulation over several flights contributed to the event. It is not an uncommon standard operating procedure for research aircraft to perform fresh water engine washes after prolonged flights in the marine boundary layer. While this is done to prevent corrosion, it certainly applies here for salt fouling as well.

Lastly, NOAA might consider borrowing the concept of Tactical Decision Aid (TDA) from Department of Defense air operations. In short, TDAs are automated programs that can poll environmental databases or utilize user input data to compare to provide guidance and highlight danger areas. To aid mission planners, satellite, meteorological model, and oceanographic data can be polled and danger areas can be graphically mapped.

5.3 Available Navy Aids for Forecasters and Mission Planners

To close this report, it is worth discussing currently available products from NRL to help forecasters and mission planners. Recently, NAAPS transitioned to FNMOC for global aerosol forecasts. Run offline on the NOGAPS meteorological fields, this first operational version of NAAPS predicts sulfate, dust, and smoke. However, a sea salt component is currently in beta testing. All of these products are available at the NRL Aerosol website (<http://www.nrlmry.navy.mil/aerosol/>). Global NOGAPS and mesoscale COAMPS® meteorology model fields can also be found at the FNMOC website (<https://www.fnmoc.navy.mil>).

The NAAPS salt component is demonstrated in Figure 18, where surface level common mode sea salt is plotted for the January 22, February 8, and February 9 flights. Clearly, on a qualitative level, the model accurately indicates large shifts in salt concentration.

In addition to model data, NRL generates a number of geostationary satellite images. All of the satellite images used in this report are taken from their quasi-operational streams. Images are primarily derived from the NRL Satellite Page (http://www.nrlmry.navy.mil/sat_products.html). Also, for the continental United States, additional products can be found at the NextSAT page (<http://www.nrlmry.navy.mil/NEXSAT.html>).

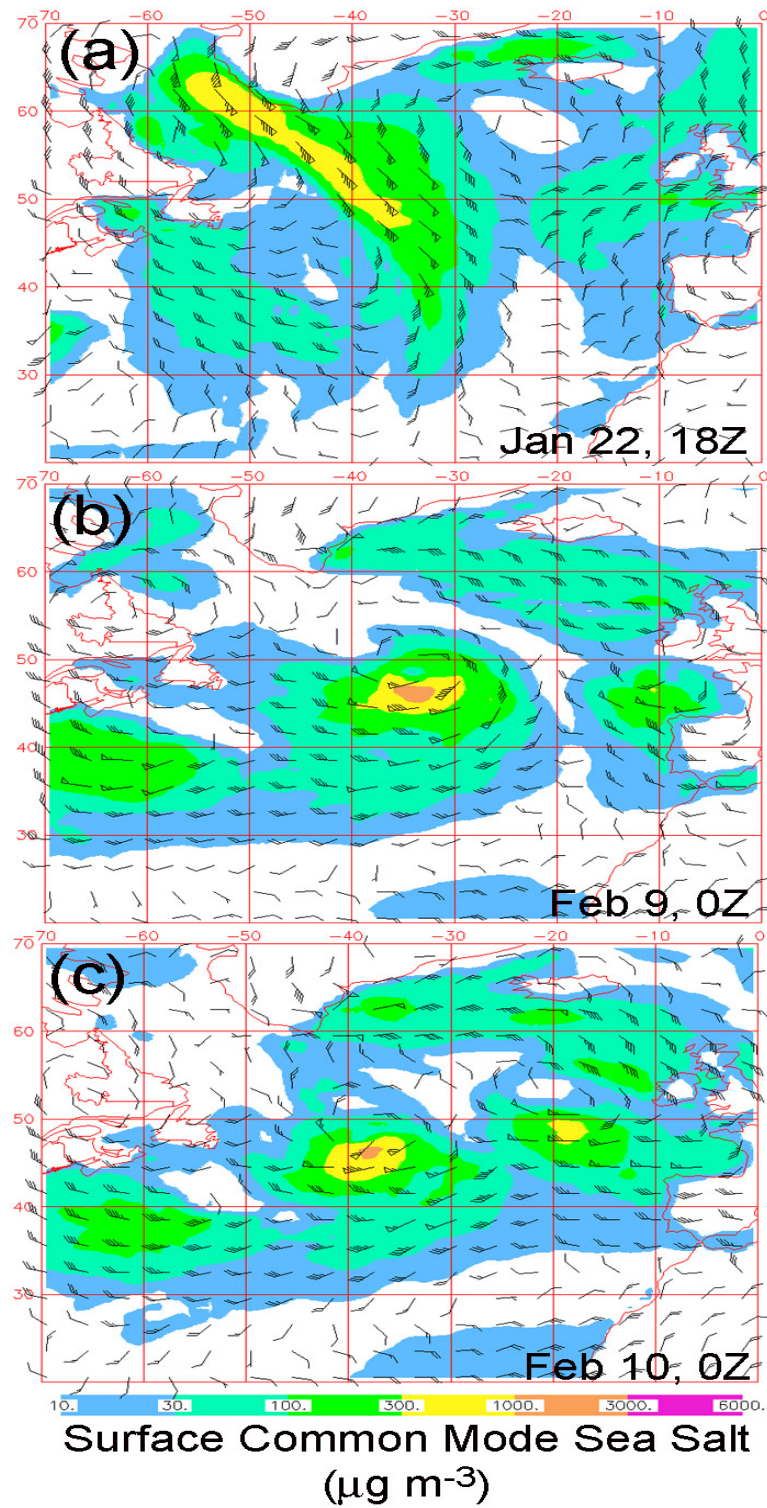


Figure 18: Navy Aerosol Analysis and Prediction System (NAAPS) surface sea salt concentration fields ($\mu\text{g m}^{-3}$) for the closest time periods for the flights on (a) January 22, (b) February 8, and (c) February 9. Overlaid is the Navy Operational Global Atmospheric Prediction System (NOGAPS) surface wind fields (kts).

6.0 SUMMARY RECOMMENDATIONS

1. High winds (>50 kts; especially >60 kts) with little precipitation can result in high concentrations of airborne sea salt particles. Even under more benign conditions, giant mode particles can reach 800 m. Under the worst of conditions, sea salt particles of this size can probably reach ~1.5 km.
2. The high-wind, dry, cold sector behind a front or southwest of an occluded system appears to be the most dangerous region in the storm for sea salt fouling. Air within this region typically experiences a long fetch over fully risen seas with extensive spume production and little precipitation to reduce aerosol loading, as well as strong inversion strengths due to a combination of dynamic surface forcing and large scale subsidence. Flight through warm, sea salt particle laden air in updrafts followed by a drying cycle in dry downdrafts likely led to a salt accretion process on the aircraft skin. While salt fouling at low levels is a concern in this region, flying at higher altitudes or closer to the storm center increases potential icing hazards. In the absence of technologies for onboard environmental assessment, careful track planning and satellite reconnaissance immediately before takeoff are the most likely means for risk mitigation.
3. There are several products available on the web that can forecast high sea salt concentrations in the atmosphere. An additional quasi-operational tool is the NRL Aerosol Analysis and Prediction System (NAAPS) surface sea salt concentration. While NAAPS currently cannot sufficiently predict salt at flight level, it does provide a reasonable warning area for flight operations.
4. WP-3D aircraft should probably be fitted with particle probes on a routine basis. But even these types of sensors can produce erroneous readings due to fouling in high concentration environments. However, by collecting this data on a regular basis, better guidelines regarding salt prone areas can be generated.
5. While we believe that the aircraft encountered a salt “event” and not that the aircraft experienced a gradual buildup over several flights, this gradual buildup hypothesis is untested and caution is warranted.
6. These extremely high sea salt particle concentrations are a previously unconsidered phenomenon in the scientific community. Additional research as to their formation and impacts is warranted.

7.0 ACKNOWLEDGMENTS

This investigation on possible meteorological influences on the unscheduled engine shutdown of the NOAA WP-3D aircraft N42RF at ~21 Z February 9, 2007, was conducted under the following programs: ONR 322 Aerosol Radiation and Microphysics (N001407wx20648), ONR 322 Large Scale Aerosol Modeling and Prediction (N001407wx20649) and NRL Base Battlespace Environment Assessment for Situational Awareness (WU 6774). The production and retrieval of archived meteorological analysis and satellite data used in this analysis required the aid of many members of NRL's staff, especially the Remote Sensing (7541) and On-Scene Systems (7542) Sections. In particular, the aid of Gary Love, F. Joseph Turk, Cristian Mitrescu, and Jeffrey Hawkins is gratefully acknowledged. We also wish to thank Carl Friehe for helpful conversations. This report was sent to Dr. Mark Stoelinga, University of Washington Atmospheric Science Department, for external review. We appreciate his time and helpful comments.

8.0 REFERENCES

- Andreas, E. L. (1998), A new sea spray generation function for wind speeds up to 32 m/s, *J. Phys. Oceanogr.* 28, 2175-2184.
- Black, P. G., E. A. D'Asaro, W. M. Drennan, et al. (2007), Air-sea exchange in hurricanes: Synthesis of observations from the Coupled Boundary Layer Air-Sea Transfer Experiment, *Bull. Amer. Meteor. Soc.* 88, 357-374.
- Blanchard, D. C., A. H. Woodcock, and R. J. Cipriano (1984), The vertical distribution of the concentration of sea salt in the marine atmosphere near Hawaii, *Tellus*, 118-125.
- Crahan, K. K., D. A. Hegg, D. S. Covert, H. Jonsson, J. S. Reid, D. Khelif, and B. J. Brooks (2004), Speciation of organic aerosols in the tropical mid-Pacific and their relationship to light scattering, *J. Atmos. Sci.* 61, 2544-2558.
- De Leeuw, G. (1990), Profiling of aerosol concentrations, particle size distributions and relative humidity in the atmospheric surface layer over the North Sea, *Tellus* 42B, 342-354.
- Exton, H. J., J. Latham, P. M. Park, M. H. Smith, and R. R. Allan (1986), The production and dispersal of maritime aerosol, In *Oceanic Whitecaps and their Role in Air-Sea exchange Processes*, E. C. Monahan and G. Mac Niocaill, eds., pp. 175-193 (D. Reidel, Norwell, Mass.).
- Fairall, C. W., K. L. Davidson, and G. E. Schacher (1983), An analysis of the surface production of sea-salt aerosols, *Tellus*, 35B, 31-39.
- Fitzgerald, J. M. (1991), Marine Aerosols: a review. *Atmos. Environ.* 25A, 533-545.
- Hodur, R. M. (1997), The Naval Research Laboratory's Coupled Ocean/Atmosphere Mesoscale prediction System (COAMPS), *Mon. Weath. Rev.* 135, 1414-1430
- Hogan, T. F., and T. E. Rosmond (1991), The description of the Navy Operational Global Atmospheric Prediction System spectral forecast system, *Month. Weath. Rev.*, 1789-1816.
- Hoppel, W., J. W. Fitzgerald, G. M. Frick, R. E. Larson, and E. J. Mack (1989), Atmospheric aerosol size distributions and optical properties found in the marine boundary layer over the Atlantic Ocean, NRL Report 9188, Naval Research Laboratory, Washington, DC, 75 pp. [NTIS AD-A210800].
- Lewis, E. R., and S. E. Schwartz (2004), Sea Salt Aerosol Production: Mechanisms, Methods, Measurements, and Models. AGU Monograph Series, number 152, Washington D.C.
- Martensson, E. M., E. D. Nilsson, G. de Leeuw, L. H. Cohen, and H. C. Hansson (2003), Laboratory simulations and parameterization of the primary marine aerosol production, *J. Geophys. Res.*, Art. No. 4297 108(D9).
- Monahan, E. C., D. E. Spiel, and K. L. Davidson (1986), A model of marine aerosol generation via whitecaps and wave disruption, In *Oceanic Whitecaps and their Role in Air-Sea exchange Processes*, E. C. Monahan and G. Mac Niocaill, eds., pp. 167-174 (D. Reidel, Norwell, Mass.).
- Porter, J., and A. D. Clarke (1997), Aerosol size distribution models based on in situ measurements, *J. Geophys. Res.* 102, 6035-6045.
- Randles, C. A., L. M. Russell, and V. Ramaswamy (2004), Hygroscopic and optical properties of organic sea salt aerosol and consequences for climate forcing, *Geophys. Res. Lett.* 31, L16108, doi:10.1029/2004GL020628.
- Reid, J. S., B. Brooks, K. K. Crahan, D. A. Hegg, T. F. Eck, N. O'Neill, G. de Leeuw, E. A. Reid, and K. D. Anderson (2006), Reconciliation of coarse mode sea-salt aerosol particle size measurements and parameterizations at a subtropical ocean receptor site, *J. Geophys. Res.* 111, D02202, doi:10.1029/2005JD006200.

- Reid, J. S., H. Jonsson, M. Smith, and A. Smirnov (2001), Evolution of the vertical profile and flux of large sea-salt particles in a coastal zone, *J. Geophys. Res.* 106, 12,038-12,053.
- Reid, J. S., and T. M. Peters (2007), Update to “Reconciliation of coarse mode sea-salt aerosol particle size measurements and parameterizations at a subtropical ocean receptor site” regarding the use of aerodynamic particle sizers in marine environments, *J. Geophys. Res.* 112, D04202, doi:10.1029/2006JD007501.
- Shapiro, M. A., and D. Keyser (1990), On the structure and dynamics of fronts, jet streams and the tropopause. Extratropical Cyclones: The Erik Palmén Memorial Volume, C. W. Newton and E. O. Holopainen, eds., Amer. Meteor. Soc., pp.167-191.
- Smirnov, A., B. N. Holben, O. Dubovic, R. Fruin, T. F. Eck, and I. Slutsker (2003), Maritime component in aerosol optical models from Aerosol Robotic Network data, *J. Geophys. Res.* 108(D1), 4033, doi:10.1029/2002JD002701.
- Smith, M. H., P. M. Park, and I. E. Consterdine (1993), Marine aerosol concentrations and estimated fluxes over the sea, *Quart. J. Roy. Meteor. Soc.* 119, 809-824.
- Tang, I. N., A. C. Tridico, and K. H. Fung (1997), Thermodynamic and optical properties of sea salt aerosols, *J. Geophys. Res.* 102, 23,269-23,275.
- Terrill, E. J., W. K. Melville, and D. Stramski (2001), Bubble entrainment by breaking waves and their influence on optical scattering in the upper ocean, *J. Geophys. Res.* 106, 16815-16823.
- Turk, F.J., and S.D. Miller (2005), Toward Improving Estimates of Remotely-Sensed Precipitation with MODIS/AMSR-E Blended Data Techniques. *IEEE Trans. Geosci. Rem. Sensing* 43, 1059-1069.
- Witek, M. L., P. J. Flatau, P. K. Quinn, and D. L. Westphal (2007), Global sea salt modeling-results and validation against multi-campaign shipboard measurements, *J. Geophys. Res.*, in press.
- Wu, J., J. J. Murray, and R. J. Lai (1984), Production and distribution of sea spray, *J. Geophys. Res.* 89, 8163-8189.

